Late Mesozoic-Cenozoic magmatism in the Lut Block: a response to the Neotethyan roll-back and continental extension

Journal:	*International Geology Review*
Manuscript ID	TIGR-2019-0194
Manuscript Type:	Special Issue
Date Submitted by the Author:	27-May-2019
Complete List of Authors:	Javidi Moghaddam, Maryam; Ferdowsi University of Mashhad Faculty of Sciences, Department of geology Karimpour, Mohammad Hassan; Ferdowsi University of Mashhad Faculty of Sciences, Department of Geology and Research Center for Ore Deposit of Eastern Iran Malekzadeh Shafaroudi, Azadeh; Ferdowsi University of Mashhad Faculty of Sciences, Department of geology and Research Center for Ore Deposit of Eastern Iran Santos, José Francisco; University of Aveiro Department of Geosciences, Department of Geosciences, Geobiotec Research Unit Corfu, Fernando ; University of Oslo, Department of Geosciences and CEED
Keywords:	Eocene magmatism, Sr-Nd isotopes, Zircon U-Pb dating, Lut Block, Iran

Late Mesozoic-Cenozoic magmatism in the Lut Block: a response to the Neotethyan roll-back and continental extension

Maryam Javidi Moghaddam[1], Mohammad Hassan Karimpour[2]*, Azadeh Malekzadeh Shafaroudi[2], Jose F. Santos[3], Fernando Corfu[4]

[1]*Department of Geology, Faculty of Science, Ferdowsi University of Mashhad, Mashhad, Iran*

[2]*Department of Geology and Research Center for Ore Deposit of Eastern Iran, Faculty of Science, Ferdowsi University of Mashhad, Mashhad, Iran*

[3]*Department of Geosciences, Geobiotec Research Unit, University of Aveiro, Portugal*

[4]*Department of Geosciences and CEED, University of Oslo, Norway*

*Corresponding author Email: karimpur@um.ac.ir

Abstract

Late Mesozoic-Cenozoic magmatic rocks constitute the main lithological units of the Lut Block and occur in an area of 60000 km^2. Our field observation from the eastern Lut (Khur region) indicate intrusive rocks occur as dike (granitoid and mafic dikes) and shallow plutons (monzonites) in the Lut Block. Volcanic rocks (basaltic andesites, andesites, trachyandesites, dacites, rhyodacites) are also abundant and are intruded into pyroclastic rocks. U–Pb zircon ages indicate that granitic-dioritic dikes and monzonite were emplaced at 44.97 to 40.86 Ma and 41.11 Ma, respectively. Granitoid dikes are high-K calc-alkaline and metaluminous and geochemically belong to I-type granitoids. Monzonites show I-type (and rarely A-type) signatures, with typical enrichments in alkalis, Zr and Ce, high $FeO_t/(FeO_t+MgO)$ ratio and depletion in Sr and Nb. Geochemical data, including major and trace elements and Sr-Nd isotopes indicate that the volcanic and intrusive rocks are products of a mantle source, presumably modified by sediment melts/fluids. The genesis of these rocks is suggested to be associated with extension above the subducting Sistan Ocean slab beneath the Lut Block. Subduction-related extension was also responsible for the high magmatic rate during Late Cretaceous–Oligocene and was associated large-scale Cu-Au mineralization in the Lut Block.

Keywords: Eocene magmatism, Sr-Nd isotopes, Zircon U-Pb dating, Lut Block, Iran.

Introduction

Widespread Late Mesozoic-Cenozoic arc magmatism accompanied subduction of Neotethyan oceanic lithosphere below the southern Eurasian margin. Such igneous rocks are common along the Alpine-Himalayan Tethyan orogenic belt, from the Alps in the west through Turkey and the Caucasus eastward into Iran, the Lhasa terrane of Tibet, and southern China. Eocene magmatic flare-up was one of the most significant magmatic events in Iran, resulting in occurrence of widespread magmatic rocks across the Iranian plateau (Berberian and King, 1981; Camp and Griffis, 1982; Schroder, 1944; Verdel et al., 2011; Moghadam et al., 2015). The flare-up magmatism seems to be behaved differently in various parts of Iran with different magmatic pulses and distinctive geochemical-isotopic signatures. The magmatic flare-up continued to Oligocene and Miocene in some segments of Iran (Fig. 1).

The magmatic flare-up is best climaxed in central Iran, in the Urumieh-Dokhtar Magmatic Belt (UDMB). The UDMB is a 50-80 km wide magmatic belt that trends NW-SE for 1000 km across Iran. The UDMB records ~ 100 Myr magmatic activity, started with late Cretaceous magmatism in southern parts and continued to the Eocene flare-up nearly in all its segments and ended with Miocene fertile magmatism in its SE parts. Temporally, the UDMB includes a thick (~ 4 km) pile of early calc-alkaline and late shoshonitic as well as adakitic rocks.

Cenozoic magmatic rocks are not only recorded in the UDMB, but instead are abundant in NW, NE and eastern Iran. In NW Iran, Eocene to Miocene mafic shoshonitic and ultrapotassic rocks are abundant and Miocene alkaline and Quaternary adakitic rocks are less widespread (e.g., Kheirkhah et al., 2009; Pang et al., 2013; Moghadam et al., 2018). In NE Iran, magmatism started with the late Cretaceous calc-alkaline granites, climaxed by Eocene high-K and adakitic magmatism and ended with Miocene-Quaternary volcanism (Shabanian et al., 2012, Alaminia et al., 2013; Moghadam et al., 2015, 2016).

In eastern Iran magmatism are different and started in late Cretaceous along with the Birjand-Sistan ocean spreading (Camp and Griffis, 1982; Tirrul et al., 1983). The magmatism is continued during the Cenozoic time at the contact of the Lut and Afghan Blocks (the Sistan suture zone). Late Cretaceous adakitic granodiorites and Paleocene-Eocene granites were emplaced in the Sistan suture zone (Zarrinkoub et al., 2010). The Eocene intrusions including Shah-Kuh and Zahedan granites have zircon U-Pb ages of ~44 to ~29 Ma (Eocene-Oligocene) (Mohammadi et al., 2016). The Sistan suture zone is also covered by a high pile of the Latest Cretaceous-Eocene volcano-sedimentary units. Widespread Eocene-Oligocene calc-alkaline magmatic activities are present both in the Sistan suture zone and to the west, in the Lut Block. Eruption of alkali basalts was also active from the Miocene to Quaternary along the suture zone and within the Lut Block (Pang et al., 2012). In this paper, we aim to study the geochronological and petrological signatures of magmatic rocks from the Lut Block.

The Lut Block, is an elongate rigid mass in Eastern Iran, bounded to the east by the Nehbandan Fault, to the west by the Nayband Fault, to the north by the Doruneh Fault, and to the south by the Jazmourian basin (Stocklin and Nabavi, 1973; Berberian and King, 1981; Karimpour and Stern, 2009). The Lut Block is underlain by the Cadomian magmatic rocks which have some exposures in its northern segments (e.g., Rossetti et al., 2015).

Extensive Late Cretaceous-Oligocene plutonism are also recorded in the Lut Block, which most of them are associated with several types of mineralization (Karimpour et al., 2012). The main Late Cretaceous-early Oligocene plutonism in the Lut blosk include the Maher-Abad, Khopik, Dehsalm, Mahoor, Sorkh-Kuh and Shah Soltan Ali intrusions (Fig. 2) (Malekzadeh Shafaroudi et al., 2012, 2015; Arjmandzadeh and Santos, 2014; Miri Beydokhti et al., 2015; Hosseinkhani et al., 2017; Nadermezerji et al., 2018). Most of these plutons are accompanied with Cu mineralization, although Au epithermal deposits are also recorded from eastern Iran (Richards et al., 2012; Abdi and Karimpour, 2013; Samiee et al., 2016).

In this paper, we focus on an outcrop of magmatic rocks from eastern Iran, the Khur pluton (Fig. 2), which host numerous occurrences of Cu±Ag±Pb±Zn vein-type mineralization. Geochemical data indicate 6.5 wt.% Cu for this intrusion. Mineralogical, geochemical as well as fluid inclusions and stable isotope studies indicate the mineralization has a magmatic source and is considered as a significant economic interest (Javidi Moghaddam et al., 2018).

Despite, the detailed studies of the economic potential of the Khur intrusion, no geochemical and geochronological studies have been performed on Khur magmatic rocks. In this study, we present the first systematic whole rocks geochemical, Sr-Nd isotopic and geochronological (zircon U-Pb) study of the Khur (E Iran) magmatic rocks. The primary goals of this paper are: 1) to understand the source and origin of the Khur magmatic rocks and to distinguish the relationship between Cu mineralization to magmatism within the Lut Block. 2) in a broader sense, to establish the timing of magmatism in E Iran using our new and compiled zircon U-Pb age results; and 3) to reveal the source and origin of the Late Cretaceous-Oligocene magmatism within the Lut Block.

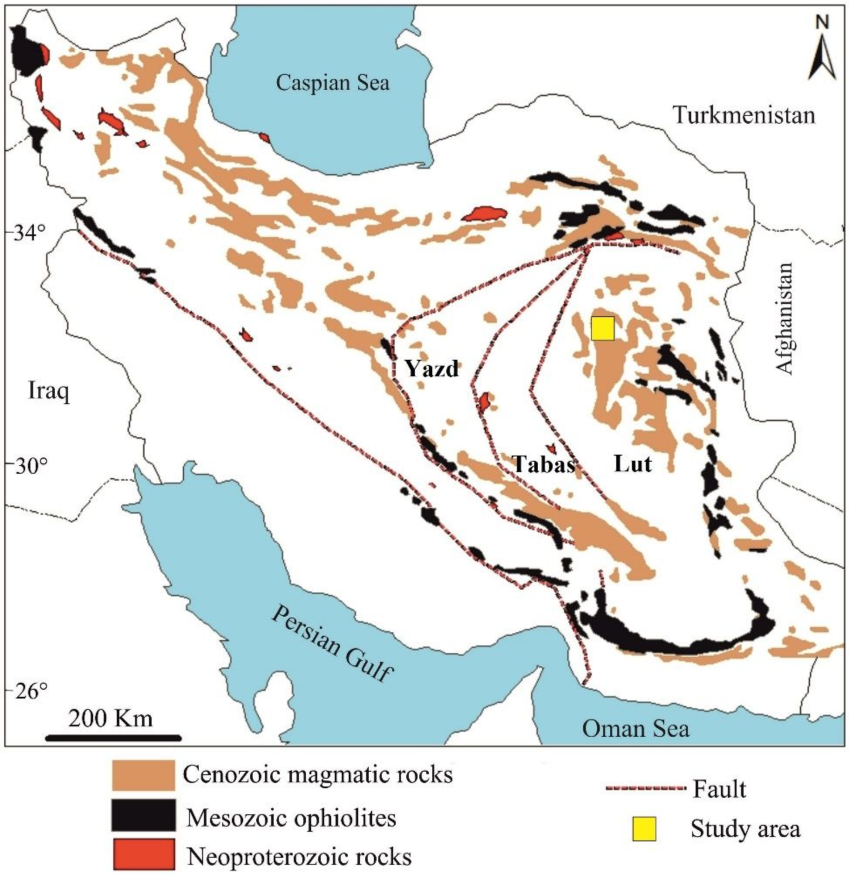

Figure 1- Simplified geological map of Iran showing the distribution of Eocene magmatic rocks and Mesozoic ophiolites in Iran (modified after Moghadam et al., 2015).

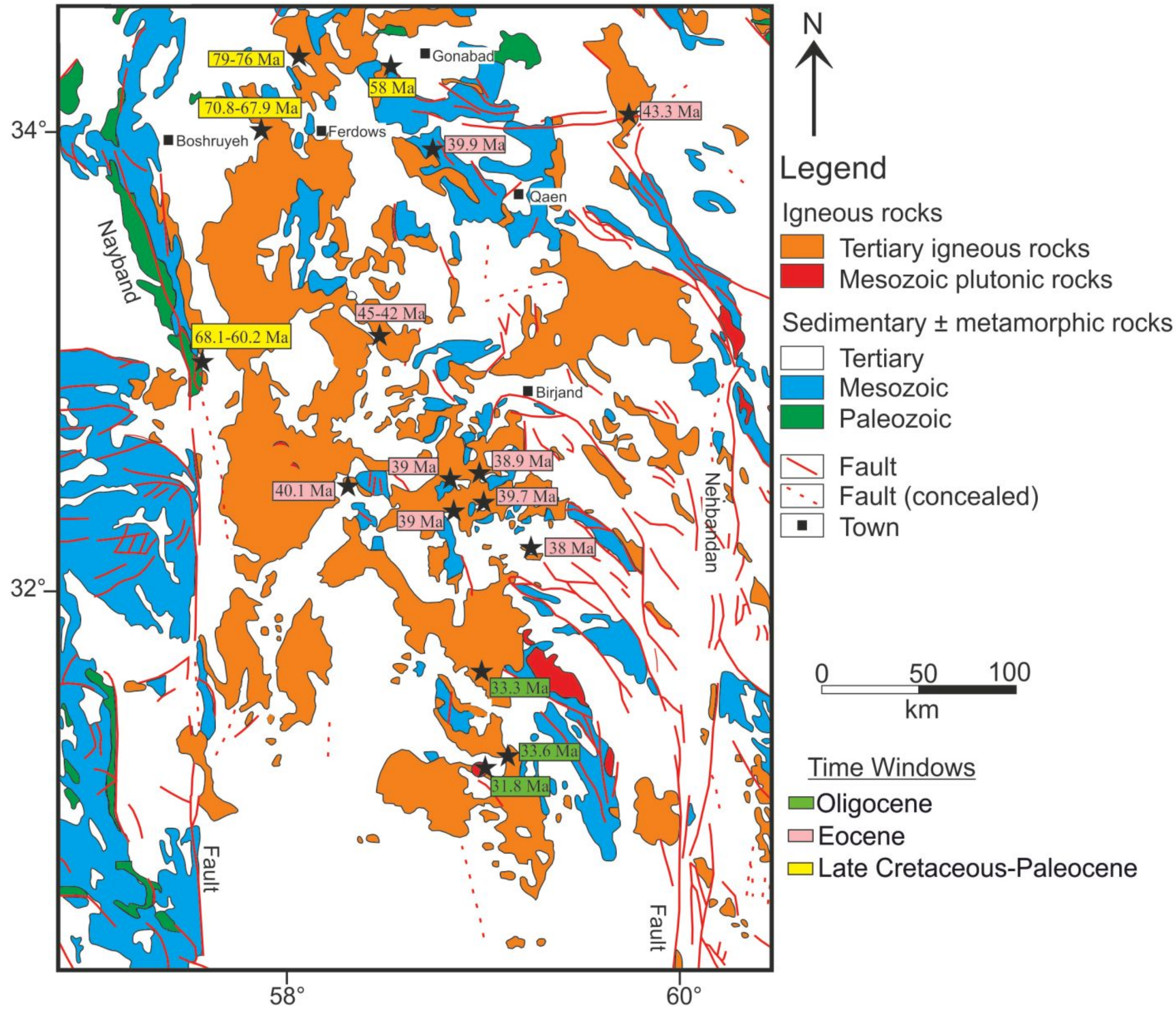

Figure 2- Major Tertiary mineralization occurrences associated with the Late Cretaceous-Oligocene I-type granitoids within the Lut Block (Jung et al, 1983; Arjmandzadeh et al. 2011; Malekzadeh Shafaroudi et al., 2012, 2015; Moradi et al., 2012; Abdi and Karimpour, 2013; Arjmandzadeh and Santos, 2014; Najafi et al., 2014; Zirjani Zadeh, 2015; Miri Beydokhti et al., 2015; Mahdavi et al., 2016; Samiee et al., 2016; Hosseinkhani et al., 2017; Nadermezerji et al., 2018; Salati et al., 2013; Javidi Moghaddam et al., 2019).

Geological setting

The oldest rocks in the Khur region include Upper Jurassic sandstones (Fig. 3). Mesozoic magmatism in this area is characterized by Eocene volcanic and intrusive rocks. Eocene volcanic rocks include andesitic to rhyolitic tuff breccias (Fig. 4a), basaltic andesites, andesites, trachyandesites, dacites and rhyodacites (Fig. 3). Andesites show Rb–Sr age of 39.3 Ma (Tarkian et al., 1983). Intrusive rocks occur as stocks and dikes. These rocks petrographically are divided into three groups: (1) monzonite, (2) granodiorite and diorite dikes, and (3) mafic rocks including gabbro and gabbrodiorite dikes. Dikes are mostly abundant in southern parts of the Khur region and have a N-S trend (Figs. 3 and 4b). The widths and lengths of these dikes vary from 0.5 to ~35 m and 20 m to 3 km, respectively (Fig. 4c and d). The presence of copper vein mineralization both at the contacts of granodiorite and diorite dikes with the volcanic-pyroclastic rocks and the presence of alteration-mineralization in dikes indicates that these dikes have triggered Cu±Ag±Pb±Zn mineralization. Mafic dikes are late-stage intrusions and show neither alteration nor mineralized and cut the granitoid dikes. Therefore, these mafic dikes are considered as post-mineralization magmatic inputs (Fig. 4e).

The Khur region is tectonically active and are characterized by local NW–SE and NE–SW strike-slip faults. The mineralized veins are localized mostly along the NW–SE faults. Veins contain bornite, chalcocite, pyrite, tennantite, galena, together with minor sphalerite and chalcopyrite as hypogene minerals and chalcocite, digenite, covellite, malachite, azurite, atacamite, hematite, and goethite as supergene minerals. Wall rock alteration occurs as narrowly-developed zones around mineralized veins and included silicification, carbonatization and argillic alteration.

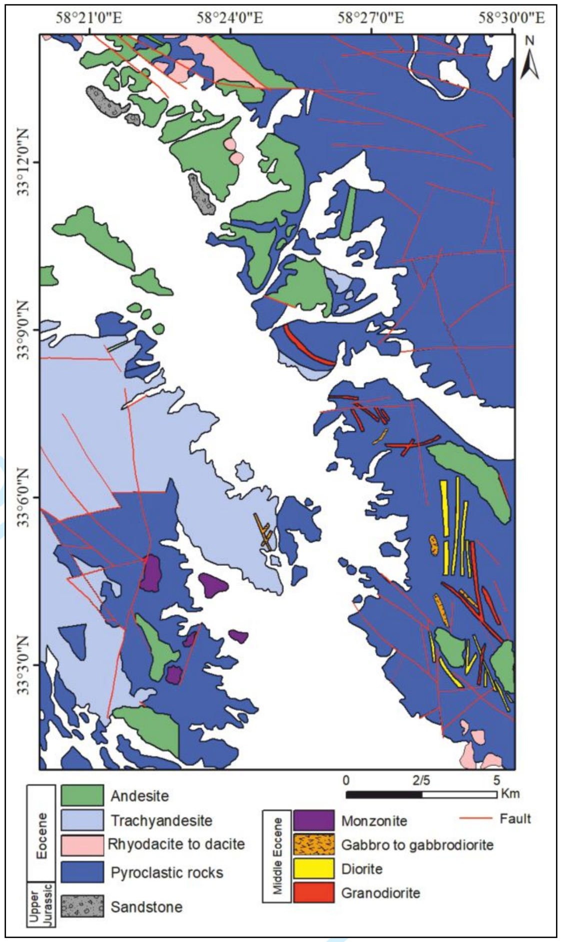

Figure 3- Simplified geological map of the Khur area (modified after 1/100000 Sarghanj geological map).

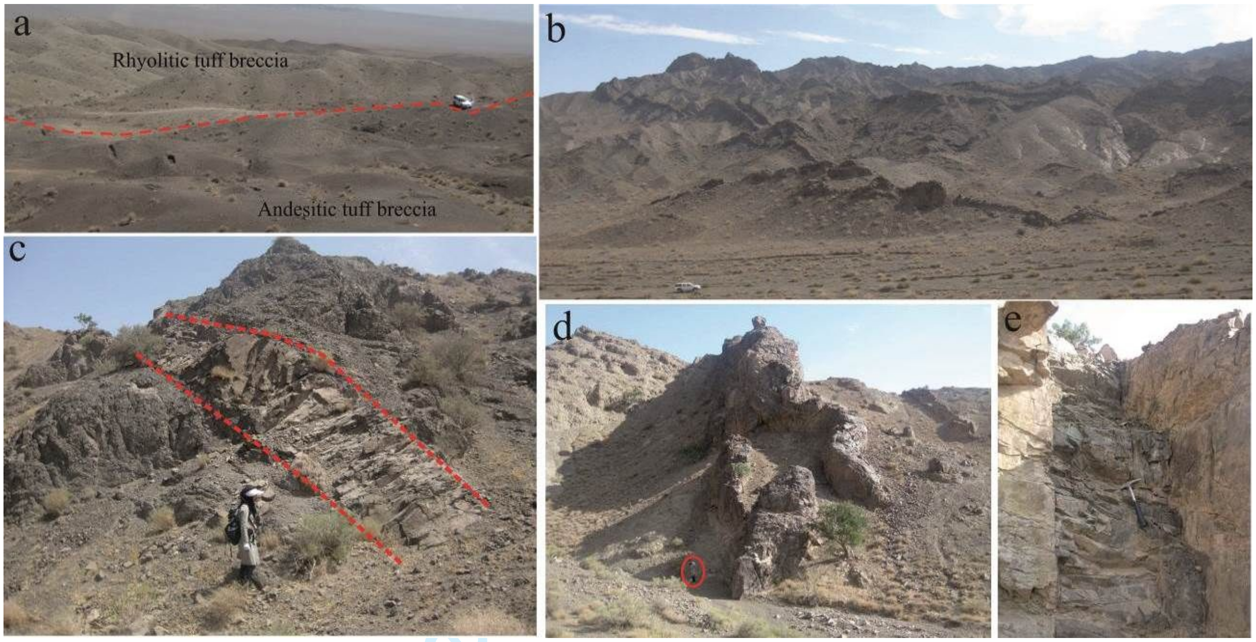

Figure 4- Field photographs of the Khur magmatic rocks. (a) Outcrops of rhyolitic and andesitic tuff breccias, (b) outcrops of dikes in the southern parts of the Khur area, (c) granodiorite dikes crosscut andesitic tuff breccias, (d) outcrops of diorite dikes, (e) gabbroic dikes crosscut granodiorite dikes.

Analytical methods

Thin sections (350 in total) from the volcanic and intrusive rocks were studied by optical microscope. Twenty-six fresh and/or least-altered samples were selected for whole rock analysis. Selected samples were crushed after removal of weathered surfaces and then grinded by an agate ball mill, in order to obtain a fine rock powder of less than 200 mesh. Major elements were determined by X-ray fluorescence spectrometry (XRF) using fused discs and the Philips PW1480 XRF spectrometer at the laboratory of Kansaran Binaloud, Mashhad, Iran. Trace and rare earth element (REE) analyses for twenty-six samples were carried out by Inductively Coupled Plasma

Mass Spectrometry (ICP-MS) following a lithium metaborate/tetraborate fusion after nitric acid total digestion at the ACME Laboratories, Vancouver, Canada.

Strontium and neodymium isotope analyses were performed for eleven whole-rock samples at the Laboratory of Isotope Geology, University of Aveiro, Portugal. The powdered samples were dissolved with a HF/HNO_3 solution in Teflon Parr acid digestion bombs at 200º C temperatures for 3 days. After evaporation of the final solution, the samples were dissolved with HCl (6N) and dried again. The elements to analyze were purified using conventional ion chromatography technique in two stages; 1) separation of Sr and REE elements in ion exchange column with AG8 50W Bio-Rad cation exchange resin; 2) purification of Nd from other lanthanide elements in columns with Ln Resin (EiChrom Technologies) cation exchange resin. All reagents used in the preparation of the samples were sub-boiling distilled, and the water produced by a Milli-Q Element (Millipore) apparatus. Sr was loaded on a single Ta filament with H_3PO_4, whereas Nd was loaded with HCl on the Ta side filament of a triple filament arrangement. $^{87}Sr/^{86}Sr$ and $^{143}Nd/^{144}Nd$ isotopic ratios were determined using a Multi-Collector Thermal Ionization Mass Spectrometer (TIMS) VG Sector 54. Data were acquired in dynamic mode with peak measurements at 1–2 V for ^{88}Sr and 0.5–1.0 V for ^{144}Nd. Sr and Nd isotopic ratios were corrected for mass fractionation relative to $^{88}Sr/^{86}Sr = 0.1194$ and $^{146}Nd/^{144}Nd = 0.7219$. During this study, the SRM-987 standard gave an average value of $^{87}Sr/^{86}Sr = 0.710261$ (±17) (N = 13; conf. lim = 95%) and JNdi-1 standard gave an average value of $^{143}Nd/^{144}Nd = 0.5120970$ (±76) (N = 13; conf. lim = 95%).

Three rock samples were selected for zircon U-Pb geochronology. We analyzed one granodiorite dike isotope dilution TIMS U–Pb age analyses. Zircons were separated by standard mineral separation techniques using a Frantz® magnetic separator and heavy liquids. The crystals were subsequently handpicked under a binocular microscope. According to optical microscopy the best quality zircon grains were cleaned with HNO_3, acetone and ultra-pure H_2O. A mixed ^{202}Pb–^{205}Pb–^{235}U tracer solution was added prior to dissolution. Chemical separation and purification of uranium and lead were performed in small Teflon® columns, according to the procedure described by Krogh (1973) and modified by Corfu (2004). Uranium and lead isotopic compositions were measured on a Finnigan MAT 262 multicollector mass spectrometer at the Department of Geosciences, University of Oslo, Norway. The samples and a mixed NBS 982Pb + U500 standard, were loaded on single rhenium filaments using a silica-gel activator and H_3PO_4. Initial Pb was corrected using Stacey and Kramers (1975) model compositions. Decay constants are from Jaffey et al. (1971). U–Pb age parameters were calculated using ISOPLOT 3 Microsoft Excel add-in (Ludwig, 2003).

Two samples of diorite dike and monzonite were prepared for U-Pb dating at the Arizona Laserchron Center using LA-ICPMS. Zircons were isolated from each rock by using standard techniques involving crushing, washing, heavy liquid and handpicking under the binocular microscope at Ferdowsi University of Mashhad. U–Pb isotope data were gathered using a New Wave 193 nm ArF laser ablation system coupled to a Nu Plasma HR inductively coupled plasma-mass spectrometer (ICP-MS) using methods described by Gehrels et al. (2008).

Petrography

Intrusive rocks

As we mentioned before, there are three types of intrusive rocks in the Khur region: 1) gabbro to gabbrodioritic dikes; 2) diorite to granodioritic dikes; and 3) monzonite.

Gabbros

Gabbros have a fine- to medium-grained granular texture with a grain size of 0.6–1.5 mm. These rocks are composed of plagioclase (labradorite) (45–50%), clinopyroxene (30–35%), olivine (5–10%), hornblende (3-5%) and accessory (<1%) magnetite and apatite. Plagioclases are slightly altered to epidote and sericite whereas clinopyroxenes (augite) are relatively fresh.

Gabbros-diorites

Gabbro-diorites have a porphyritic texture with medium-grained groundmass. These rocks contain plagioclase (15–20 vol.%), clinopyroxene (augite) (5– 7 vol.%), hornblende (3–5 vol.%) and olivine (2-3 vol.%). The accessory minerals are apatite, magnetite and pyrite. Some plagioclases are slightly replaced by sericite, chlorite and calcite.

Diorites

These intrusive rocks display porphyritic texture. Phenocrysts consist of medium to large-grained (0.6 mm–2.2 cm) plagioclase (30–35%), K-feldspar (1–3%), hornblende (7–10%), pyroxene (3–5%) and biotite (1–2%). Accessory minerals include magnetite and zircon plus some minor quartz in some samples. Euhedral to subhedral plagioclase (andesine–labradorite) phenocrysts are normally zoned and slightly altered to sericite, epidote and clay minerals. Clinopyroxene (augite) is replaced by carbonate, and hornblende shows alteration into chlorite, epidote and calcite.

Granodiorites

These rocks have a porphyritic texture with phenocrysts of plagioclase (20–25%) (range in size from 0.1 mm –2 cm), K-feldspar (5–10%) (0.1–0.4 mm), quartz (8–10%) (0.1–0.2 mm), hornblende (6–8%) (0.2 mm–1 cm), biotite (7–10%) (0.2 mm–1 cm) and <2% accessory minerals (zircon+ apatite+ magnetite). Plagioclase phenocrysts range in composition from oligoclase to andesine (An<20–An40) and are moderately to strongly altered into clay minerals, calcite and epidote. Euhedral hornblende phenocrysts have been altered to chlorite, epidote and calcite. Hornblende is occasionally replaced by opaque minerals along the crystal rims and the cleavages. Subhedral biotite phenocrysts are altered to chlorite and epidote.

Monzonites

Monzonites have porphyritic and glomero-porhyritic textures. Phenocrysts are 15–20% plagioclase (0.8–1.5 mm), 15–18% K-feldspar (0.2–0.4 mm), 5-7% hornblende (0.7mm-1cm) and 3–5% quartz (0.1–0.5 mm). Apatite and magnetite are also present. Plagioclase is andesine (An30-An45) and is slightly altered to sericite, epidote and clay minerals. Hornblende appears as euhedral crystals and show alteration into epidote, chloritized and calcite.

Volcanic rocks

The Khur volcanic rocks cover a wide compositional range from basaltic andesites, to trachyandesites, andesites, dacites and rhyodacites. The most relevant mineral assemblages and textural features are described below.

Rhyodacites

Rhyodacites have a porphyritic texture and contains up to 35 vol.% phenocrysts (0.2-1 mm in diameter). Phenocrysts are euhedral plagioclase (albite- oligoclase) (8-10 vol.%), K-feldspar (6-8 vol.%), quartz (3-5 vol.%), euhedral to subhedral biotite (4-5 vol.%), and hornblende (1-2 vol.%). These minerals occur also in the groundmass along with the glass. Accessory minerals are magnetite and apatite.

Dacites

These rocks have porphyritic and microlitic textures. Phenocrysts in these rocks consist of plagioclase with a composition from albite to oligoclase (8–10 vol.%), K-feldspar (2–4 vol.%), biotite (4-5 vol.%), quartz (3-5 vol.%) and hornblende (2–3 vol.%). The groundmass is dominated by plagioclase, quartz and glass. Feldspar phenocrysts are locally altered to sericite and clay minerals. Biotite and hornblende are slightly altered to chlorite. Accessory minerals include apatite. The glassy groundmass shows trace of devitrification with development of fine-grained quartz and feldspars.

Andesites

Andesitic rocks display a porphyritic texture and normally contain > 25 vol.% of phenocrysts (0.8-4 mm in diameter) in a glassy groundmass. Phenocrysts include 10–12 vol.% plagioclase (oligoclase-andesine), 4–5 vol.% hornblende, 3-5 vol.% biotite and 2-3 vol.% clinopyroxene. The groundmass is dominated by plagioclase and cryptocrystalline materials. Accessory minerals include magnetite and apatite. Hornblende has been occasionally replaced by chlorite and calcite. Euhedral to subhedral plagioclase phenocrysts show zonation and have slightly altered to sericite, clay minerals and calcite.

Trachyandesites

These rocks have a trachytic texture. Phenocrysts are plagioclase (12–14 vol. %), hornblende (3–5 vol. %) and K-feldspar (5–7 vol. %). The same minerals are also present in the groundmass. Apatite and magnetite are common accessory minerals. Plagioclase is andesine and show alteration into sericite and calcite.

Basaltic andesites

Basaltic andesites have porphyritic and glomeroporhyritic textures. These rocks contain plagioclase (andesine–labradorite) (10–15 vol. %), pyroxene (5–7 vol. %), hornblende (3–5 vol. %) and olivine (2–3 vol. %). The groundmass is dominated by plagioclase, pyroxene and altered glass. Some hornblende phenocrysts have been replaced by carbonate. Plagioclases have been altered into epidote and calcite.

Whole rock geochemistry

Major and trace elements

Major and trace elements composition of intrusive and volcanic rocks is presented in Table 1. In addition, we have used the bulk rock geochemical results of volcanic rocks which have been published by Salim (2012) for the central segment of the Khur area. Total alkalies *vs* silica (TAS, Middlemost, 1985) and Zr/TiO_2 *vs* SiO_2 (Winchester and Floyd, 1977) diagrams were chosen for a lithological classification. In these diagrams, dikes fall in the granodiorite, diorite, gabbro-diorite and gabbroic fields. Our sample from the Khur stock plot in monzonite field, whereas volcanic rocks show tendency to plot in rhyodacite-dacite, andesite-trachyandesite and basaltic andesite fields (Fig. 5a and b).

In the K_2O versus SiO_2 diagram (Peccerillo and Taylor, 1976) (Fig. 5c), dikes and volcanic rocks plot in high-K calc-alkaline and shoshonitic fields. In the A/NK (molecular $Al_2O_3/(Na_2O+K_2O)$) versus A/CNK (molecular $Al_2O_3/(CaO+ Na_2O+ K_2O)$) diagram (Maniar and Piccoli, 1989) (Fig. 5d), dikes and monzonite are metaluminous with alumina saturation index < 1.1, which is the upper limit for the I-type granitoids (Chappell and White, 2001). The Khur rocks are magnesian to ferroan and plots in the alkali-calcic and calc-alkalic fields on the modified alkali-lime index diagram (Frost et al., 2001) (Fig. 6a and b).

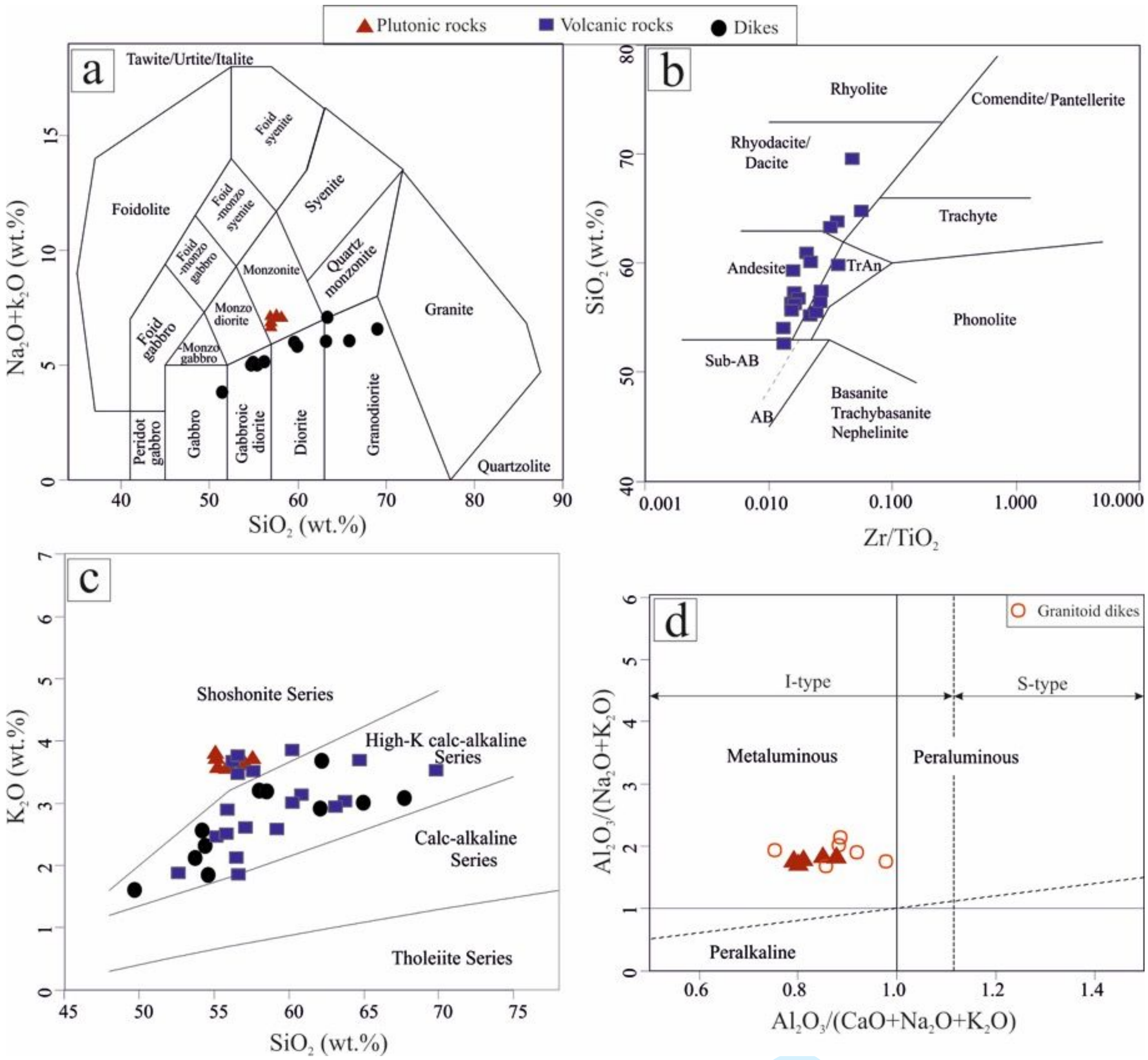

Figure 5- (a) Classification diagrams for the geochemical classification of the Khur samples. (a) Na_2O+ K_2O *vs* SiO_2 (TAS) diagram (Middlemost, 1985), (b) Zr/TiO_2 *vs* SiO_2 (Winchester and Floyd, 1977), (c) K_2O *vs* SiO_2 diagram (Peccerillo and Taylor, 1976), (d) $Al_2O_3/Na_2O + K_2O$ (molar) *vs* $Al_2O_3/(CaO + K_2O + Na_2O)$ diagram (molar) (Maniar and Piccoli, 1989). The field boundaries between S-type and I-type granite are from Chappell and White (1992).

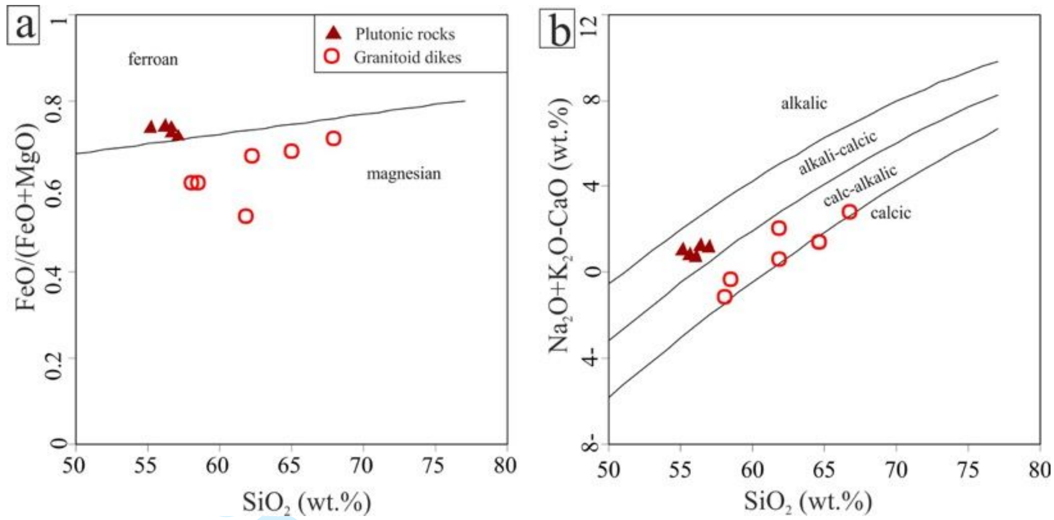

Figure 6- (a) $FeO_t/(FeO_t+ MgO)$ *vs* SiO_2 diagram for the classification of the Khur felsic rocks The ferroan-magnesian boundary is from Frost et al. (2001). (b) Modified alkali-lime index (MALI) (Na_2O + K_2O/CaO) *vs* SiO_2. The alkalic, alkali-calcic, calc-alkalic, and calcic boundaries are after Frost et al. (2001).

On a primitive mantle-normalized multi-elements plot (Fig. 7a, c, e and g; Sun and McDonough, 1989), the composition of all intrusive and volcanic rocks are similar to the rocks from the subduction-related environments (Pearce and Peate, 1995; Villagómez et al., 2011). In this diagram, the Khur rocks show enrichment in large ion lithophile elements (LILEs: Cs, Rb, Ba, and K) and other incompatible elements (Th and U), and depletion in high field strength elements (HFSEs: Nb and Ti).

Volcanic rocks are represented by high Sr and low Nb, Ta and Ti contents, which suggested to be due to the absence of plagioclase but presence of Fe–Ti oxides in the melting residue of the source area for their parental magmas (Martin, 1999). Negative anomalies in P may be related to apatite fractionation (Fig. 7e).

In volcanic rocks (trachyandesite) and samples from monzonite, Ba displays depletion compared to other LILEs (Fig. 7c and g). This differential behavior of Ba compared to other LILEs may be due to the addition of a sediment component from the subducted slab to the melt reservoir of these rocks (Borg et al., 1997; Leat et al., 2003). Also, in the volcanic (trachyandesite) and monzonite samples, Zr, P, Ce, K, Rb displays enrichment along ith slight depletion in Nb (Fig. 7c and g). In chondrite-normalized REE diagrams (Boynton, 1984), intrusive and extrusive rocks have similar patterns (Fig. 7b, d, f and h). Igneous rocks are characterized by enrichment in light rare-earth elements (LREEs) relative to heavy rare earth elements (HREEs). The La_N/Yb_N ratios of dikes, volcanic and plutonic rocks range between 5.37-8.71, 6.97-19.23 and 7.6-7.7, respectively. These ratios are smaller compared to the adakitic magmas (with La_N/Yb_N >30 e.g., Martin, 1987) with garnet in the source.

Except for one sample (sample D69, Eu/Eu* =0.733), dikes have no Eu anomalies (Eu/Eu* = 0.825-1) (Fig. 7b; Table 1). Volcanic rocks have negligible negative Eu anomalies, with Eu/Eu* of 0.83 to 0.89, except for a rhyodacite (sample S-P-35, Eu/Eu* =1.035) which displays a slight positive Eu anomaly (Fig. 7f; Table 1).

Trachyandesites and monzonite have negative Eu anomalies, with Eu/Eu* of 0.703 to 0.762 and 0.629 to 0.754, respectively (Fig. 7d and h; Table 1). Normally, a negative Eu anomaly indicates magma differentiation due to fractional crystallization of plagioclase (Henderson, 1984). However, at high fO_2 conditions Eu will be present mainly as Eu^{3+} and, therefore, only small amount of Eu^{2+} will be available for incorporation in plagioclase (Hezarkhani, 2006). The negative Eu anomaly and low Sr contents in the monzonite and trachyandesites indicate fractional crystallization of plagioclase was a prevailed mechanism.

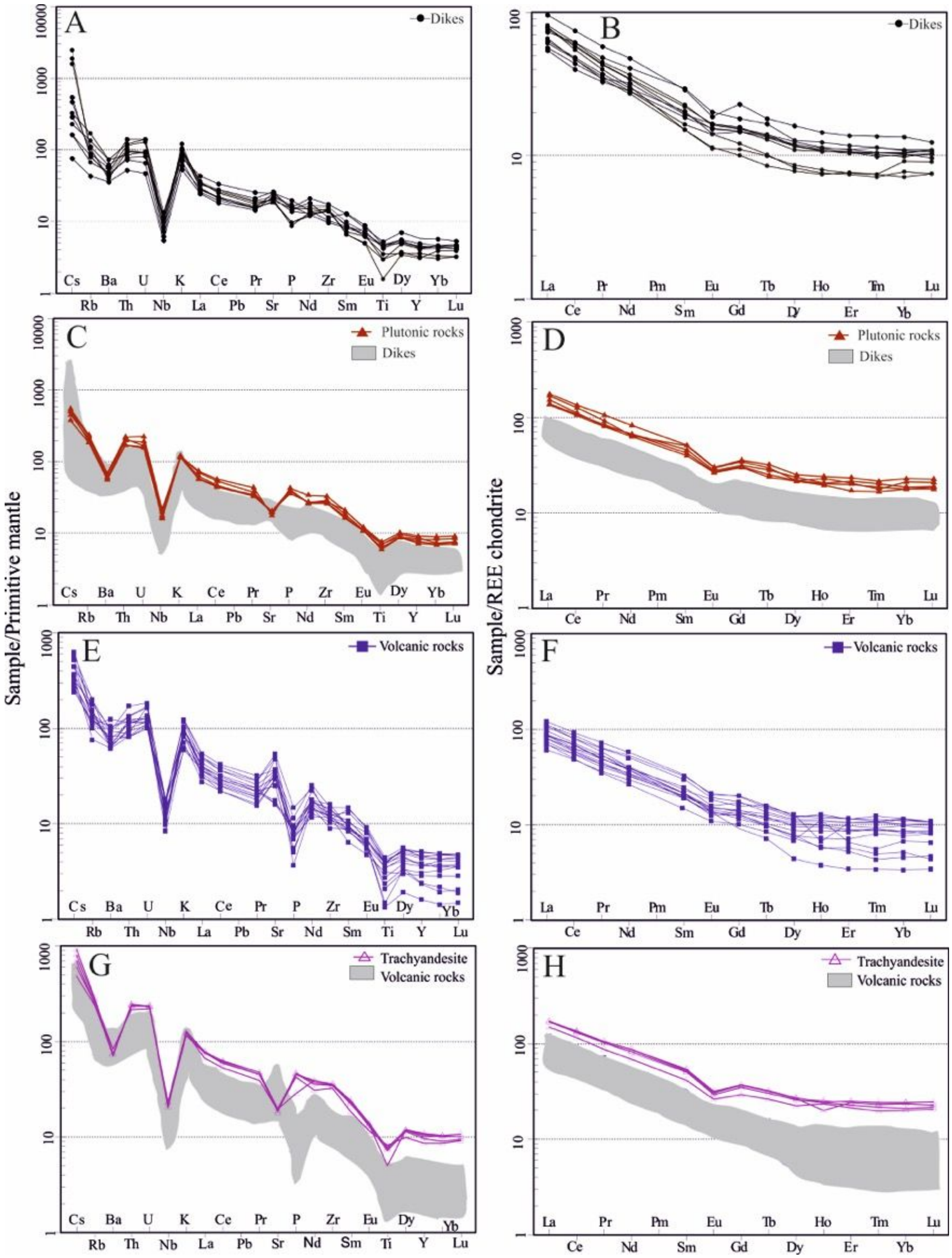

Figure 7- primitive-mantle-normalized trace elements (normalizing values after Sun and McDonough (1989)) and chondrite-normalized rare earth elements (normalizing values after

Boynton (1984)) patterns for the Khur dikes (a–b), the monzonite (c–d), the volcanic rocks (e–f) and trachyandesite rocks (g–h).

Whole rock Sr–Nd isotopes

Initial $^{87}Sr/^{86}Sr$ and εNd values were calculated considering a 45 Ma age for diorite dikes and a 41 Ma age for the other lithologies (Table 2). Granitoid dikes are represented by initial $^{87}Sr/^{86}Sr$ ratios ranging from 0.70476 to 0.70498, whilst εNdi values vary between +0.4 and +3.1 (Table 2). Two analyzed mafic dikes gave initial $^{87}Sr/^{86}Sr$ ratios of 0.70474 and 0.70475, and εNdi values of +1.7 and +2.2 (Table 2). Initial $^{87}Sr/^{86}Sr$ ratios of monzonites are +0.70477 and +0.70478; with εNdi of +3.16 (Table 2).

Trachyandesites have $(^{87}Sr/^{86}Sr)_i$ and εNdi values of 0.70469 to 0.70498 and +1.8 to +3.0, respectively (Table 2). Initial $^{87}Sr/^{86}Sr$ ratio and εNdi value for basaltic andesite are in the range of 0.70496 and +0.8, respectively (Table 2). In the εNdi versus $(^{87}Sr/^{86}Sr)_i$ diagram (Fig. 8), all samples fall to the right of the so-called mantle array and show tendency toward the continental crust. According to the position of the studied samples, the parental magmas probably were derived from partial melting of a metasomatized (enriched) mantle wedge in a supra-subduction zone environment. Nd isotopic composition of the magmatic samples also attest that these rocks record assimilation of the continental materials during their ascent and/or emplacement.

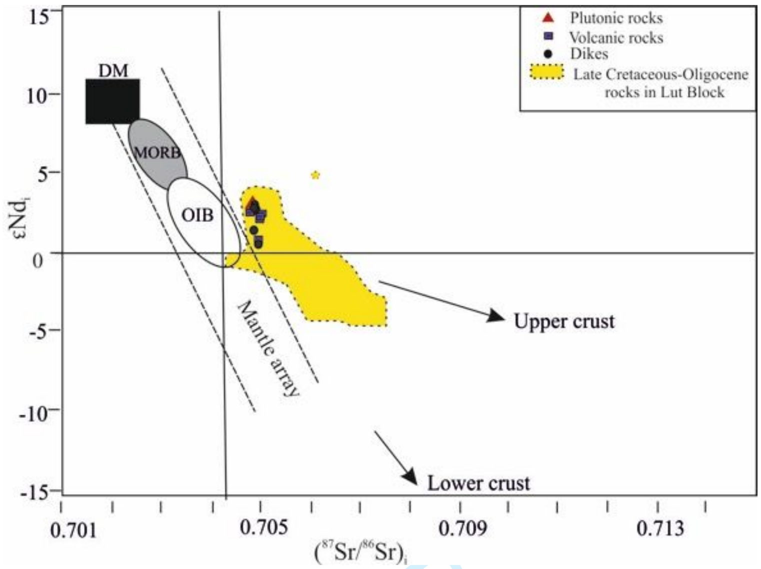

Figure 8- Diagram of εNd(i) vs. ($^{87}Sr/^{86}Sr$)i for Khur rocks. Reference data sources: upper continental crust (Taylor and McLennan, 1985); lower continental crust (Rollinson, 1993; Rudnick, 1995), MORB (Sun and McDonough, 1989; Rollinson, 1993), DM (McCulloch and Bennett, 1994), OIB (Vervoort et al., 1999) and mantle array (Gill, 1981; Wilson, 1989; McCulloch and Bennett, 1994). MORB: Mid-ocean ridge basalts; DM: Depleted mantle; OIB: Ocean-island basalts. Data for Late Cretaceous-Oligocene I-type granitoids from Jung et al, 1983; Arjmandzadeh et al. 2011; Moradi et al., 2012; Malekzadeh Shafaroudi et al., 2015; Abdi and Karimpour, 2013; Salati et al., 2013; Arjmandzadeh and Santos, 2014; Najafi et al., 2014; Zirjani Zadeh, 2015; Miri Beydokhti et al., 2015; Samiee et al., 2016; Hosseinkhani et al., 2017; Nadermezerji et al., 2018.

Zircon U-Pb geochronology

We have dated three rock samples from Khur area. Zircon U-Pb results for these igneous rock samples (D33 (diorite dike), SH6 (monzonite) and D4 (granodiorite dike)) are shown in Tables 3 and 4 and illustrated in Figs. 8 and 9.

Diorite dike

Zircon grains from diorite dikes are euhedral to subhedral (with length of ~60 to 450 µm), transparent and mostly show oscillatory growth zoning, suggesting their magmatic origin (Hanchar and Hoskin, 2003). Rim-core structure is absent. Thirteen dated spots show weighted mean $^{206}Pb/^{238}U$ age of 44.97 ± 0.74 Ma ((MSWD=0.44) (Fig. 9a and b).

Monzonite

Sample SH6 contains two groups of zircons. In group 1, zircon crystals are mostly euhedral with oscillatory growth zoning and lengths of ~70 to 500 µm. Based on eleven analyses on 8 zircon grains, the weighted mean $^{206}Pb/^{238}U$ age is 41.14 ± 0.43 Ma ((MSWD=1.6) (Fig. 1). In the other group, zircon grains show short prismatic forms (average crystal lengths of ~50–100 µm) and have subhedral to euhedral shapes. They are colorless and transparent. The weighted mean $^{206}Pb/^{238}U$ age of these zircons is 543.13 ± 12 Ma (MSWD=5.3, n=9) (Fig 9c and d). These zircons are xenocrystic zircons.

Granodiorite dike

Zircon crystals in this sample are euhedral to subhedral and short prismatic (see inset in Fig 10). Rim-core structures are common in zircons (Table 4). The youngest data obtained from a single zircon tip defines a concordia age of 40.86 ± 0.44 (MSWD=0.93). All other analyses reflect the different ages of cores and zircon xenocrysts. Two of the lines shown in Fig.10 project to upper intercept ages of *ca* 557 and 1911 Ma, which are typical ages in the Cadomian basement, but Paleoproterozoic inheritance is also obvious.

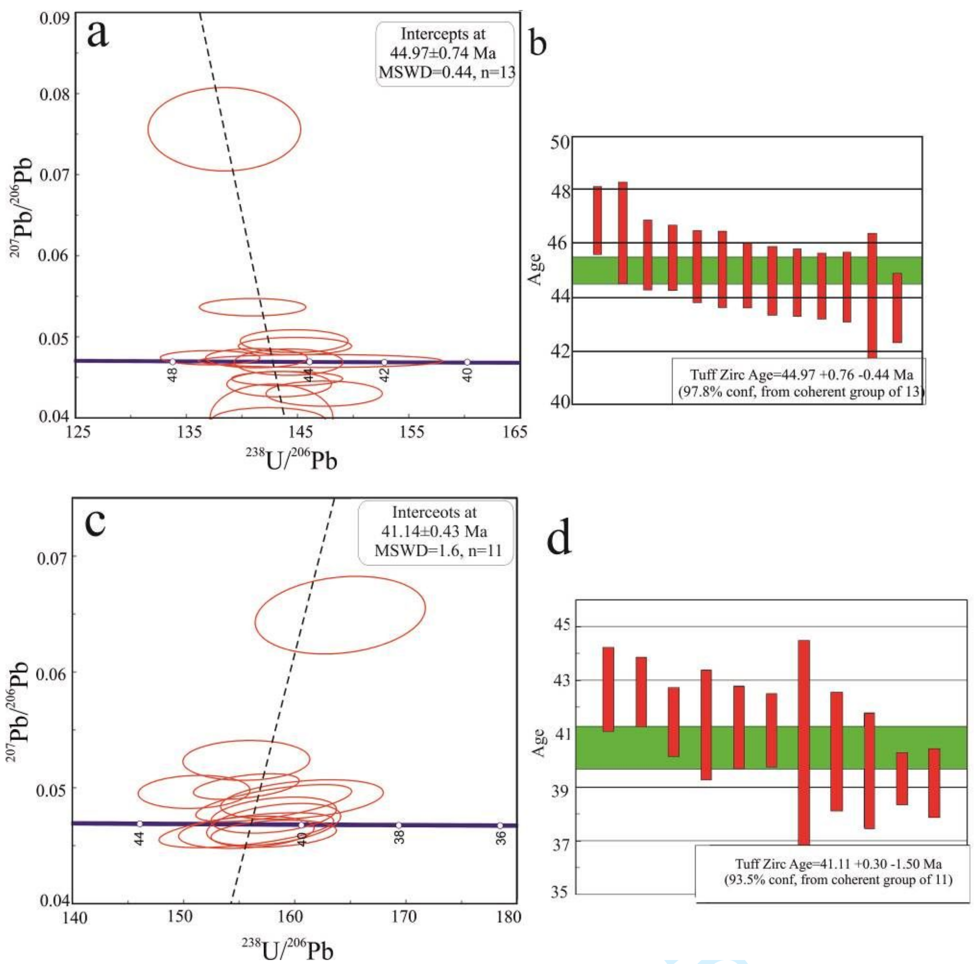

Figure 9- U–Pb inverse concordia diagrams (a, c) and average age plots (b,d) for the diorite dike (D33), above, and the monzonite (SH6), below.

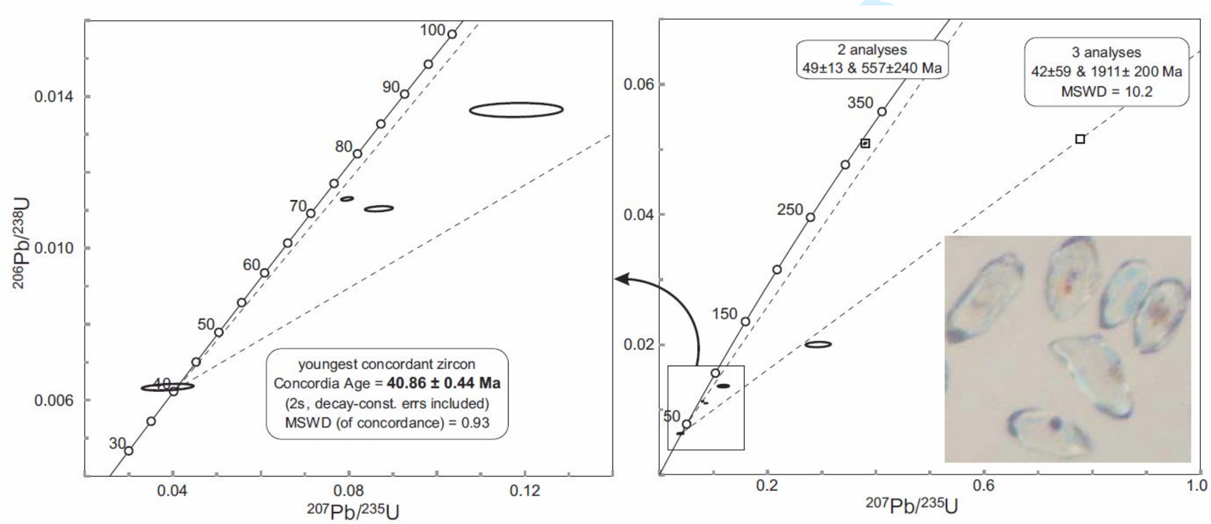

Figure 10- U–Pb Concordia diagrams for zircon in the granodiorite dike (D4). Inset shows some typical zircon grains.

Discussion

Magma source and petrogenesis

Our geochemical and isotopic data indicate that the Khur magmatic rocks are related to the melting of a metasomatized mantle wedge above a subduction zone, and show clear contamination with the Iranian continental crust. We believe these rocks should be resulted from melting, assimilation, storage and homogenization (MASH) processes in the middle crust. Assimilation of crustal materials is clear in sample SH-6 which contain abundant late Neoproterozoic-Cambrian zircons. Late Neoproterozoic-Cambrian rocks are widespread in Iran and is suggested to make the middle-lower crust of Iran (Hassanzadeh et al. 2008; Moghadam et al., 2017).

We suggest the Khur rocks should from in a continental subduction zone. All samples plot well above the MORB–OIB array and follows trend of the mantle enrichment in a Th/Yb vs. Ta/Yb diagram (Fig. 11a). The high Th/Yb ratios in these magmas may be characteristic of a metasomatized mantle source, enriched during subduction of oceanic crust. Rare earth elements and Th do not show mobility in subduction fluids, but instead sediment melts can have high concentration of these elements (Elliott et al., 1997). The aqueous fluids released from the subducting slab plays an important role in the transport of incompatible elements from the downgoing slab to the sub-arc mantle (Hermann et al., 2006). Addition of melt from sediments or altered oceanic crust (AOC) to the mantle wedge will cause positive anomalies of U and Th in magmas (Fan et al., 2003). We suggest sediment-related metasomatism in the mantle wedge has played the most important role in the origin of the monzonite and trachyandesites (Fig. 11b), which increased U, Th, Zr, Ti and REEs anomalies.

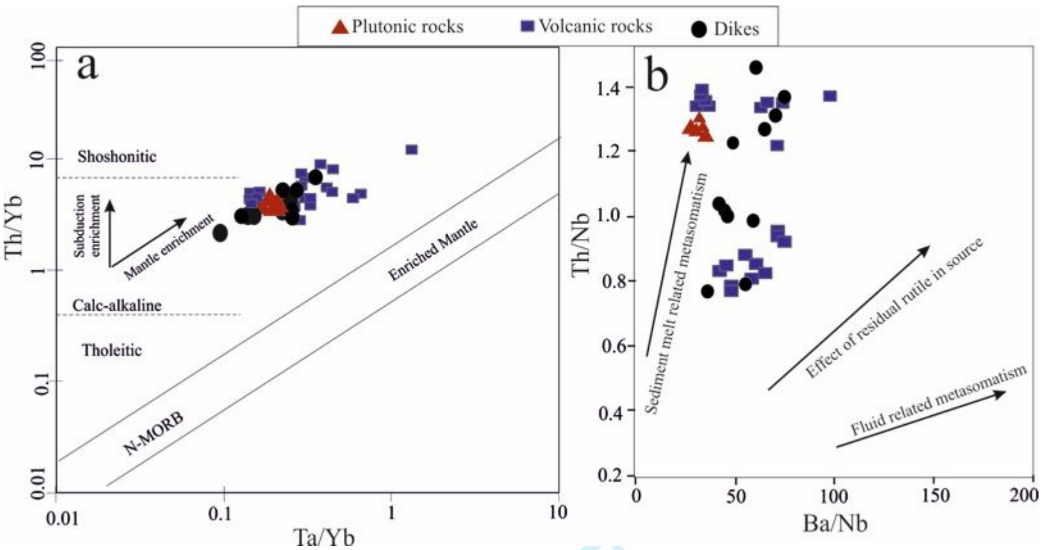

Figure 11- (a) Th/Yb vs. Ta/Yb (Pearce and Peate, 1995) and (b) Th/Nb vs. Ba/Nb (Ersoy et al., 2010) diagrams for the Khur rocks.

In Th *vs* Ta diagram from Schandl and Gorton (2002), all the samples of the Khur area plot in the field of active continental margins (Fig. 12a). Monzonites and trachyandesites plot at the boundaries of the Volcanic Arc Granite (VAG) and Within Plate Granite (WPG) fields whereas dikes and volcanic rocks generally fall in Volcanic Arc Granite domain (Fig. 12b and c).

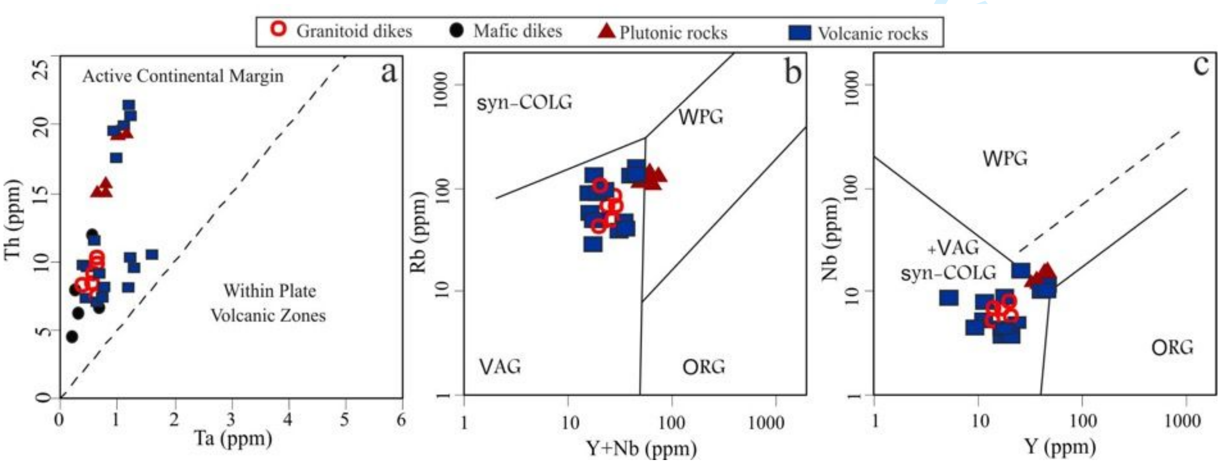

Figure 12- Tectonomagmatic discrimination diagram for the Khur rocks (a) Ta vs. Th (Schandl and Gorton, 2002), (b) Nb+Y vs. Rb and (b) Y vs. Nb (Pearce et al., 1984). WPG, within plate granites; VAG, volcanic arc granites; ORG, ocean ridge granites; syn-COLG, syncollisional granites.

In the Y and Nb versus 10000*Ga/Al discrimination diagrams (Whalen et al., 1987), the monzonite fall in the I-type and S-type domain (Fig. 13a and b). In contrast, in the Zr and Ce versus 10000*Ga/Al diagram of Whalen et al. (1987), these rocks plot in the A-type domain (Fig. 13c and d). All granitoid dikes generally fall in the I-type and S-type domains (Fig. 13). Highly siliceous S-type granites are typically strongly peraluminous with A/CNK value much higher than 1.1 (Chappell and White, 1992, 2001; Clemens et al., 2011). The granitoid dikes have A/CNK values below 1.1. Additionally, the P_2O_5 trend shows a negative correlation with SiO_2 (not show here) which is considered an important criterion for distinguishing I-type granites from S-type granites. In agreement with the I-type characteristics of granitoid rocks, specifically the $(^{87}Sr/^{86}Sr)_i$ values for I-type granitoids of Chappell and White (1974) these rocks have $(^{87}Sr/^{86}Sr)_i$ values below 0.708.

Compared to typical I-type granites, A-type granites are distinguished by high Na_2O+K_2O, high Fe(total)/Fe(total)+Mg (ferroan granites) and Ga/Al ratios, high abundances of LILE, HFSE (especially Nb and Y), high Zr (commonly >300 ppm), Ga and REE^{3+}, and low abundances of Ba, Sr and Eu, features (e.g. Loiselle and Wones, 1979; Collins et al., 1982; Whalen et al., 1987; King et al., 1997; Rämö et al., 2002).

The monzonite is mainly ferroan and alkali-calcic. This rock has chemical compositions that are typical of A-type granites, including high Zr, Ce, total FeOt/MgO and low Sr. In contrast to A-type granites, however, this rock has low Nb, Ga, Y, Na_2O+K_2O, low Ga/Al ratios and no significant depletion in Eu.

The transitional nature of a number of geochemical indicators implies that the tectono-magmatic setting was not a simple subduction zone. We suggest a transitional tectonic setting (syn- to post-collision) of the region during the Eocene because of the closure of the Sistan Sea between the Lut and Afghan Blocks.

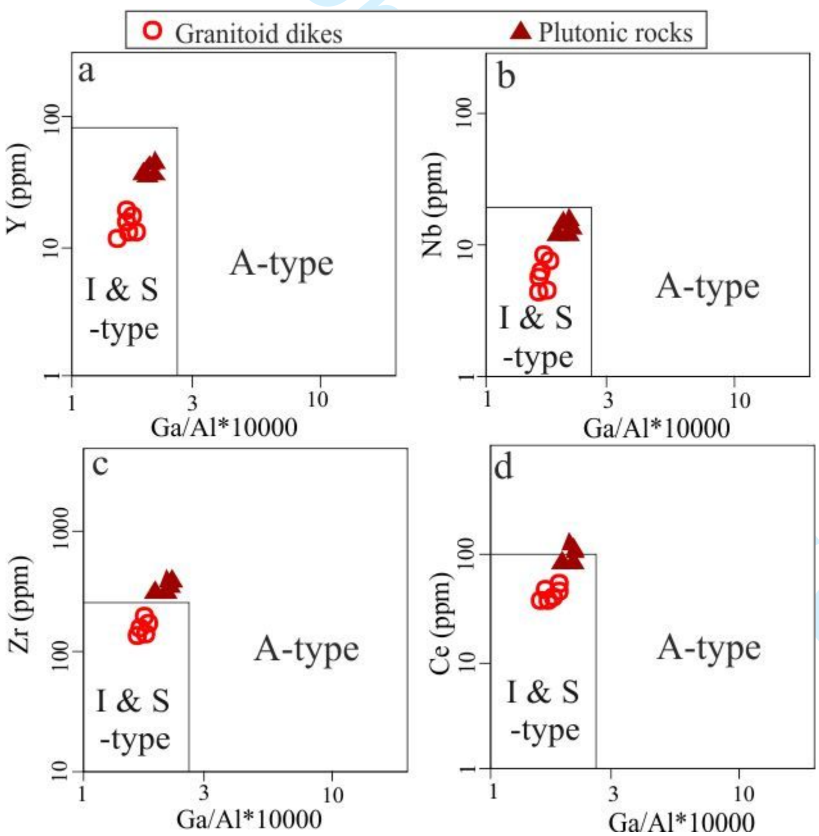

Figure 13- (a) Yb, (b) Nb, (d) Zr, and (e) Ce vs. 10,000 Ga/Al discrimination diagrams for Khur rocks (Whalen et al., 1987).

Late Cretaceous–Oligocene magmatism in E Iran and their importance

Magmatism in the Lut Block lasted from Late Cretaceous at ~77 Ma to Late Oligocene at ~22 Ma. The magmatism periods in the Lut Block can be divided into three stages (Fig. 2): 77–60 Ma (Late Cretaceous to Late Paleocene), 52–38 Ma (Early to Middle Eocene) and 33-22 Ma (Oligocene). Cretaceous-Late Paleocene magmatic rocks occur in west to northwestern parts of the Lut Block. Early to Middle Eocene rocks mostly occur in northern to central parts of the Lut Block. Finally, the Oligocene magmatic rocks are abundant in the central and southern segments of the Lut Block (Fig. 2). The composition of intrusive rocks in the Lut Block varies from diorite, monzonite, quartz monzonite and granodiorite. The volcanic rocks have basaltic, andesitic, dacitic and rhyolitic compositions.

Late Cretaceous-Oligocene granitoids are high-K calc-alkaline to slightly shoshonitic. These rocks are classified as oxidant I-type granitoids. These granitoids have initial $^{87}Sr/^{86}Sr$ ratios of 0.7043–0.7078 and εNd(i) values of +4.88 to -6.43. Most rocks fall to the right of the so-called mantle array in the εNdi versus $(^{87}Sr/^{86}Sr)_i$ diagram (Fig. 8) and suggests mantle melts with different degrees of crustal assimilation were responsible for the genesis of these rocks. So, mantle have crucial role in genesis of these rocks. Cu and Au are highly compatible in mantle rocks within sulfide phases (Fleet et al., 1996; Ballard et al., 2002). In this regard, a higher proportion of mantle component involved in the high-K calc-alkaline to slightly shoshonitic magma indicates a higher potential for Cu–Au mineralization for these magmatic rocks.

Tectonic implications

The Lut Block consists of a pre-Jurassic metamorphic basement, Jurassic sedimentary rocks, and several generations of late Mesozoic and Cenozoic intrusive and/or volcanic rocks (Camp and Griffis, 1982; Tirrul et al., 1983). Inherited zircon U-Pb data show Neoproterozoic–Cambrian ages of 557 Ma to 543 Ma while some grains also point to Paleoproterozic ages (1911 Ma), possibly detrital inheritance. Therefore, new U-Pb analyses of zircons with inherited cores from the Khur area support that crust of the Lut Block is composed of inherited continental fragments with Gondwanan affiliation as is common in the eastern Arabian shield.

Different geodynamic models have been proposed for the tectonic and magmatic evolution of the Lut Block, but its paleotectonic setting has remained highly controversial. Base on Cretaceous ophiolites the Sistan paleo-Ocean (a N–S-trending branch of Neotethys) is considered to have existed between the Lut and Afghan Blocks. The Sistan Ocean was opened in the Early Cretaceous (Babazadeh and Wever, 2004), but the mechanism and timing of ocean closure are indeterminate.

Some workers suggest eastward subduction beneath the Afghan Block (Camp and Griffis, 1982; Tirrul et al., 1983) or while others consider westward subduction beneath the Lut Block (Zarrinkoub et al., 2012). In contrast, Arjmandzadeh et al. (2011) propose simultaneous eastward and westward subduction. Also, geodynamic models of eastward intra-oceanic subduction have been proposed by Saccani et al. (2010). Pang et al. (2013) propose a post-collision system as lithospheric removal and asthenospheric upwelling associated with extensional collapse of the east Iranian ranges.

Pang et al. (2013) suggested that the Lut–Afghan collision occurred in the the Late Cretaceous, as inferred by the emplacement of ~86 Ma adakitic plutons and ~55 Ma A-type granites in the suture zone (Zarrinkoub et al., 2010), and considered the Eocene–Oligocene magmatism as post-collisional. Camp and Griffis (1982) and Tirrul et al. (1983) proposed that the Lut and Afghan Blocks collided with each other in the Middle Eocene, as evidenced by the onset of deformation of the Sefidabeh forearc basin deposits in the suture zone. They considered the Eocene–

Oligocene magmatism as syn- to postcollisional. One point for all of proposed models is that the rotation of the Lut Block is not considered.

Two of the significant events in the magmatic record of the Lut Block are almost regular process in reducing the age of magmatism from northern to southern and the absence of linear or curved magmatic belt. Base on geochemical data, Eocene–Oligocene magmatic rocks in Iran have an orogenic signature. Relative to linear or curved magmatic belts in the Urumieh–Dokhtar magmatic arc in southwestern Iran and the Alborz ranges in northern Iran, the Eocene–Oligocene magmatic rocks in the Lut–Sistan region are spread over a diffuse province of ~300 km × 400 km, which might require a different tectonomagmatic explanation.

Berberian (1973) proposed that the Lut Block behaved rigidly, and it has been argued that the Block underwent a large anticlockwise rotation in response to the collision between India and Eurasia (Besse et al., 1998; Bagheri and Stampfli, 2008). Davoudzadeh et al. (1981) postulated a counter-clockwise rotation by 135˚ of the Lut Block between the Triassic and Middle Tertiary. According to paleomagnetic data from Upper Jurassic Bidou Formation, Mattei et al. (2014) proposed large counter-clockwise rotations in the Central-East-Iranian Microcontinent (CEIM) that occurred in two distinct phases, during the Early Cretaceous (with an average amount of ≈30˚) and after the Middle–Late Miocene (with an average amount of ≈35˚) (Fig. 14). However, there isn't agreement about angle value and time of rotation.

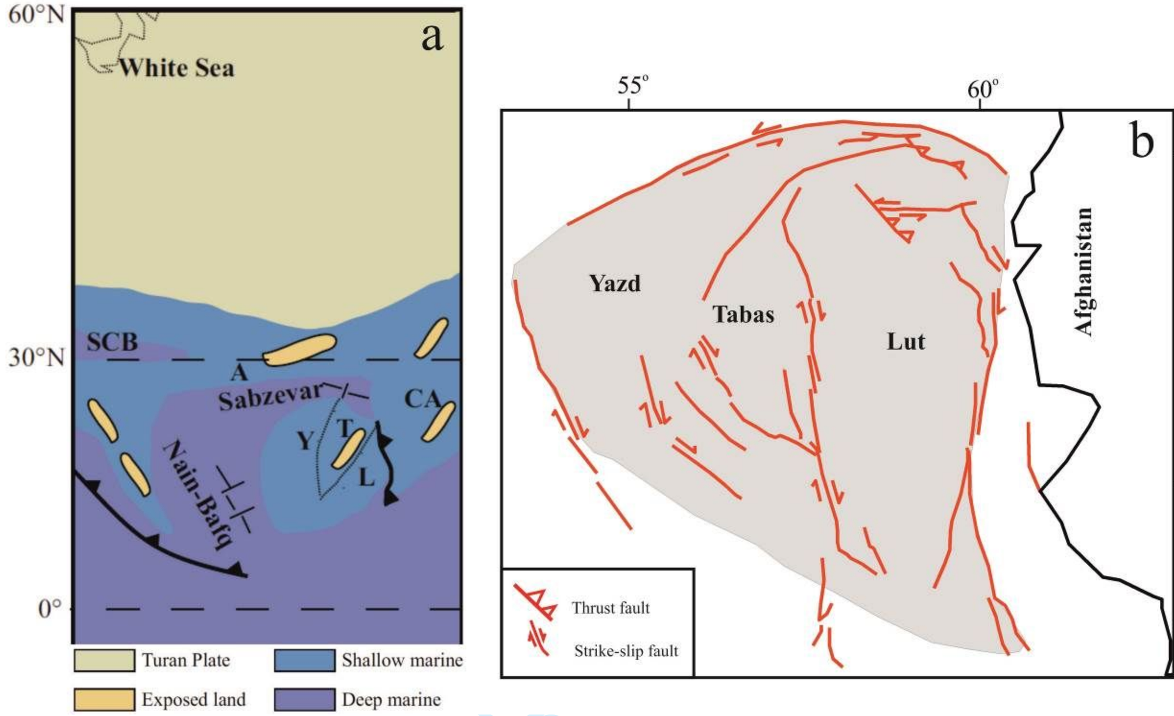

Figure 14- Paleogeographic reconstructions of the Central-East Iranian Microcontinent (CEIM) (a) 90 Ma (Mattei et al., 2014) and (b) now. Y = Yazd; T = Tabas; L = Lut; A = Alborz; SCB = Southern Caspian Basin; CA = Central Afghanistan.

The approximate concurrency of Late Cretaceous–Oligocene magmatic flare-up and rotation of the Lut Block is a considerable factor. It is possible that the Sistan Ocean was subducted beneath the Lut Block and the Lut Block and Afghan Block collided, synchronously with rotation of the Lut Block. According to this hypothesis, the similar geochemistry of I-type granitoids, the almost regular process in reducing the age of magmatism and nonlinear distribution of magmatic rocks are predictable.

Conclusion

The studied Middle Eocene intrusions consist of high-K calc-alkaline granitoid dikes (syn-mineralization), shoshonitic monzonite (non-mineralization), and mafic dikes (post-mineralized).

These igneous rocks are approximately similar in terms of their major, trace and rare earth element geochemical characteristics. The transitional nature revealed by a number of geochemical indicators suggests that Khur igneous rocks formed at the tectonic transition from of syn to post-collision extensional setting. The magmatic rocks of the Khur area are considered to have formed by partial melting of a metasomatized mantle wedge enriched by Sistan subduction with low-degrees of assimilated crust, specifically fragments of Gondwanan crust and subducted sediments.

The Late Cretaceous-Oligocene I-type granitoids in the Lut Block are characteristically high-K calcalkaline to slightly shoshonitic, likely formed by partial melting of a subduction-modified upper mantle in a syn to post-collisional extension-related zone due to the closure of the Sistan Sea between the Lut and Afghan Blocks and synchronous with rotation of the Lut Block. This magmatism was responsible for most of the large-scale Cu-Au mineralization events in the Lut Block.

Acknowledgments

The Research Foundation of Ferdowsi University of Mashhad, Iran, supported this study (Project No. 22731.3). The authors wish to thank Mrs. Sara Ribeiro (Laboratório de Geologia Isotópica da Universidade de Aveiro) for the TIMS analysis of Sr ans Nd isotopes and for the guidance and assistance during sample preparation in the clean room. Sr and Nd isotope analyses were financially supported by the Portuguese Foundation for Science and Technology, through project Geobiotec (UID/GEO/04035/2013).

References

Abdi, M., and Karimpour, M.H., 2013, Petrochemical characteristics and timing of Middle Eocene granitic magmatism in Kooh-Shah, Lut Block, Eastern Iran: Acta Geologica Sinica, v. 87, no 4, p. 1032–1044.

Alaminia, Z., Karimpour, M.H., Homam, S.M., and Finger, F., 2013, Themagmatic record in the Arghash region (northeast Iran) and tectonic implications: International Journal of Earth Sciences, v. 102, p. 1603–1625.

Arjmandzadeh, R., Karimpour, M.H., Mazaheri, S.A., Santos, J.F., Medina, J., and Homam, S.M., 2011, Sr–Nd isotope geochemistry and petrogenesis of the Chah-Shaljami granitoids (Lut Block, Eastern Iran): Asian Earth Sciences, v. 41, no. 3, p. 283–296.

Arjmandzadeh, R., and Santos, J.F., 2014, Sr–Nd isotope geochemistry and tectonomagmatic setting of the Dehsalm Cu–Mo porphyry mineralizing intrusives from Lut Block, eastern Iran: International Journal of Earth Sciences (Geologische Rundschau), v. 103, no. 1, p. 123–140.

Babazadeh, S.A., and de Wever, P., 2004, Early Cretaceous radiolarian assemblages from radiolarites in the Sistan Suture (eastern Iran): Geodiversitas, v. 26, no. 2, p. 185–206.

Bagheri, S., and Stampfli, G.M., 2008, The Anarak, Jandaq and Posht-e-Badam metamorphic complex in central Iran: new geological data, relationships and tectonic implications: Tectonophysics, v. 451, p. 123–155.

Ballard, J.R., Palin, J.M., and Campbell, I.H., 2002, Relative oxidation states of magmas inferred from Ce (IV)/Ce (III) in zircon: application to porphyry copper deposits of northern Chile: Contributions to Mineralogy and Petrology, v. 144, no. 3, p. 347–364.

Berberian, M., 1973, The Seismicity of Iran: Preliminary Map of Epicentres and Focal Depths: Geological Survey of Iran, scale 1:2 500 000, 1 sheet.

Berberian, M., and King, G.C., 1981, Towards a paleogeography and tectonic evolution of Iran: Canadian journal of Earth Sciences, v. 18, p. 210–265.

Besse, J., Torcq, F., Gallet, Y., Ricou, L.E., Krystyn, L., and Saidi, A., 1998, Late Permian to Late Triassic palaeomagnetic data from Iran: Contrains on the migration of the Iranian Block through the Tethyan Ocean and initial destruction of Pangea: Geophysical Journal International, v. 135, p. 77–92.

Borg, L.E., Clynne, M.A., and Bullen, T.D., 1997, The variable role of slab-derived fluids in the generation of a suite of primitive calc-alkaline lavas from the southernmost Cascades, California: The Canadian Mineralogist, v. 35, p. 425–452.

Boynton, W.V., 1984, Geochemistry of the rare earth elements: meteorite studies, Rare Earth Element Geochemistry: Amsterdam, Elsevier, p. 63–114.

Camp, V.E., and Griffis, R.J., 1982, Character, genesis and tectonic setting of igneous rocks in the Sistan suture zone, eastern Iran: Lithos, v. 15, no 3, p. 221–239.

Chappell, B.J., and White, A.J.R., 1974, Two contrasting granite types: Pacific Geology, v. 8, no. 173– 174.

Chappell, B.W., and White, A.J.R., 1992, I- and S- type granites in the Lachlan fold belt: transactions of the royal society of Edinburg, Earth Sciences, v. 83, p. 1–26.

Chappell, B.W., and White, A.J.R., 2001, Two contrasting granite type: 25 years later: Australian Journal of Earth Sciences, v. 48, no. 4, p. 489–499.

Clemens, J.D., Stevens, G., and Farina, F., 2011, The enigmatic sources of I-type granites: the peritectic connexion: Lithos, v. 126, no. 3–4, p. 174–181.

Collins, W.J., Beams, S.D., White, A.J.R., and Chappell, B.W., 1982, Nature and origin of A-type granites with particular reference to southeastern Australia: Contributions to Mineralogy and Petrology, v. 80, p. 189–200.

Corfu, F., 2004, U–Pb age, setting and tectonic significance of the anorthosite–mangerite–charnockite–granite suite, Lofoten-Vesterålen, Norway: Journal of Petrology, v. 56, p. 2081–2097.

Davoudzadeh, M., Soffel, H., Schmidt, K., 1981, On the rotation of the Central-East-Iran microplate. Journal of Paleontology (3): 180-192.

Elliott, T., Plank, T., Zindler, A., White, W. and Bourdon, B., 1997, Element transport from slab to volcanic front at the Mariana arc: Journal of Geophysical Research, v. 102, no. B7, p. 14991–15019.

Ersoy, E. Y., Helvacı, C., and Palmer, M. R., 2010, Mantle source characteristics and melting models for the early-middle Miocene mafic volcanism in western Anatolia: implications for enrichment processes of mantle lithosphere and origin of K-rich volcanism in post-collisional settings: Volcanology and Geothermal Research, v. 198, no. 1-2, p. 112–128.

Fan, W., Gue, F., Wang, Y. J., and Lin, G., 2003, Late Mesozoic calc-alkaline volcanism of postorogenic extension in the northern Da Hinggan Mountains, northeastern China: Volcanology and Geothermal Research, v. 121, no. 1, p. 115–135.

Fleet, M.E., Crocket, J.H., and Stone, W.E., 1996, Partitioning of platinum group elements (Os, Ir, Ru, Pt, Pd) and gold between sulfide liquid and basalt melt: Geochimica et Cosmochimica Acta, v. 60, p. 2397–2412.

Frost, B.R., Arculus, R.J., Barnes, C.G., Collins, W.J., Ellis, D.J., and Frost, C.D., 2001, A geochemical classification of granitic rocks: Petrology, v. 42, p. 2033–2048.

Gehrels, G.E., Valencia, V.A., and Ruiz, J., 2008, Enhanced precision, accuracy, efficiency, and spatial resolution of U–Pb ages by laser ablation–multicollector– inductively coupled plasma-mass spectrometry: Geochemistry, Geophysics, Geosystems, v. 9, no. 3, p. 1–13.

Gill, J.B., 1981, Orogenic Andesites and Plate Tectonics: New York, Springer, v. 16, 392 p.

Hanchar, J.M., and Hoskin, P.W.O., 2003, Zircon: Reviews in Mineralogy and Geochemistry, v. 53, p. 1–500.

Hassanzadeh, J., Stockli, D.F., Horton, B.K., Axen, G.J., Stockli, L.D., Grove, M., Schmitt, A.K., and Walker, J.D. 2008, U-Pb zircon geochronology of late Neoproterozoic-Early Cambrian granitoids in Iran: Implications for paleogeography, magmatism, and exhumation history of Iranian basement: Tectonophysics, v. 451, p. 71–96.

Henderson, P., 1984, Rare Earth Element Geochemistry: Amsterdam, Elsevier, 510 p.

Hermann, J., Spandler, C., Hack, A., and Korsakov, A. V., 2006, Aqueous fluids and hydrous melts in high-pressure and ultra-high pressure rocks: implications for element transfer in subduction zones: Lithos, v. 92, no. 3, p. 399–417.

Hezarkhani, A., 2006, Petrology of the intrusive rocks within the Sungun Porphyry Copper Deposit, Azerbaijan, Iran: Asian Earth Sciences, v. 25, no. 6, p. 1–15.

Hosseinkhani, A., Karimpour, M.H., Malekzadeh Shafaroudi, A., and Santos, J.F., 2017, U-Pb geochronology and petrogenesis of intrusive rocks: Constraints on the mode of genesis and timing of Cu mineralization in SWSK area, Lut Block: Geochemical Exploration, v. 177, no. 6, p. 11–27.

Jaffey, A.H., Flynn, K.F., Glendenin, L.E., Bentley, W.C., and Essling, A.M., 1971, Precision measurement of half-lives and specific activities of 235U and 238U: Physical Review Section C, Nuclear Physics, v. 4, p. 1889–1906.

Javidi Moghaddam, M., Karimpour, M.H., Ebrahimi Nasrabadi, K., Haidarian Shahri, M.R., and Malekzadeh Shafaroudi, A., 2018, Mineralogy, Geochemistry, Fluid Inclusion and Oxygen

Isotope Investigations of Epithermal Cu ± Ag Veins of the Khur Area, Lut Block, Eastern Iran: Acta Geologica Sinica, v. 92, no. 6, p. 1139–1156.

Javidi Moghaddam, M., Karimpour, M.H., Malekzadeh Shafaroudi, A., Santos, J.F., and Mendes, M.H., 2019, Geochemistry, Sr-Nd isotopes and zircon U-Pb geochronology of intrusive rocks: Constraint on the genesis of the Cheshmeh Khuri Cu mineralization and its link with granitoids in the Lut Block, Eastern Iran: Geochemical exploration, v. 202, p. 59–76.

Jung, D., Keller, J., Khorasani, R., Marcks, Chr., Baumann, A., and Horn, P., 1983, Petrology of the Tertiary magmatic activity the northern Lut area, East of Iran. Ministry of Mines and Metals, GSI, Geodynamic Project (geotraverse) in Iran, no. 51, p. 285–336.

Karimpour, M.H., Malekzadeh Shafaroudi, A., Stern, C.R., and Farmer, L., 2012, Petrogenesis of Granitoids, U–Pb zircon geochronology, Sr–Nd isotopic characteristic and important occurrence of Tertiary mineralization within the Lut Block, Eastern Iran: Economic Geology, v. 4, no. 1, p. 1–27 (in Persian with English abstract).

Karimpour, M.H., and Stern, C.R., 2009, Advance spaceborne thermal emission and reflection radiometer (ASTER) mineral mapping to discriminate high sulfidation, reduced intrusion related, and iron oxide gold deposits, eastern Iran: Applied Sciences, v. 9, p. 815–825.

Kheirkhah, M., Allen, M., and Emami, M., 2009, Quaternary collision magmatism from the Iran/Turky borderlands: Volcanology and Geothermal Research, v. 182, no. 1–2, p.1–12.

King, P.L., White, A.J.R., Chappell, B.W., and Allen, C.M., 1997, Characterization and origin of aluminous A-type granites from the Lachlan Fold Belt, Southeastern Australia: Petrology, v. 38, no. 3, p. 371–391.

Krogh, T.E., 1973, A low contamination method for hydrothermal decomposition of zircon and extraction of U and Pb for isotopic age determinations: Geochimica et Cosmochimica Acta, v. 37, p. 485–494.

Leat, P.T., Smellie, J.L., Millar, I.L., and Larter, R.D., 2003, Magmatism in the South Sandwich arc: London, Geological Society, p. 285–313.

Loiselle, M.C., and Wones, D., 1979, Characteristics and origin of anorogenic granites: Geological Society of America, Abstracts with Programs 11, no. 7, 468 p.

Ludwig, K.R., 2003, Users manual for Isoplot 3.00: Berkeley Geochronology Center Special Publication 4, 70 p.

Mahdavi, A., Karimpour, M.H., Mao, J., Haidarian Shahri, M.R., Malekzadeh Shafaroudi, A. and Li, H., 2016, Zircon U–Pb geochronology, Hf isotopes and geochemistry of intrusive rocks in the Gazu copper deposit, Iran: Petrogenesis and geological implications: Ore geology Reviews, v. 72, p. 818–837.

Malekzadeh Shafaroudi, A., Karimpour, M.H., and Stern, C.R., 2012, Zircon U–Pb dating of Maherabad porphyry copper–gold prospect area: evidence for a late Eocene porphyry- related metallogenic epoch in east of Iran: Economic Geology, v. 3, p. 41–60 (in Persian with English abstract).

Malekzadeh Shafaroudi, A., Karimpour, M.H., and Stern, C.R., 2015, The Khopik porphyry copper prospect, Lut Block, Eastern Iran: Geology, alteration and mineralization, fluid inclusion, and oxygen isotope studies: Ore geology Reviews, v. 65, no. 2, p. 522–544.

Maniar, P.D., and Piccoli, P.M., 1989, Tectonic discrimination of granitoids: Geological Society of America Bulletin, v. 101, no. 5, p. 635–643.

Martin, H., 1987, Petrogenesis of Archaean trondhjemites, tonalites and granodiorites from eastern Finland: major and trace element geochemistry: Petrology, v. 28, p. 921–953.

Martin, H., 1999, The adakitic magmas: modern analogues of Archaean granitoids: Lithos, v. 46, no.3, p. 411–429.

Mattei, M., Cifelli, F., Muttoni, G., and Rashid, H., 2014, Post-Cimmerian (Jurassic–Cenozoic) paleogeography and vertical axis tectonic rotations of Central Iran and the Alborz Mountains: Asian Earth Sciences, no.102, p. 92-101.

McCulloch, M.T., and Bennett, V.C., 1994, Progressive growth of the Earth's continental crust and depleted mantle: Geochemical constraints: Geochimica et Cosmochimica Acta, v. 58, p. 4717–4738.

Middlemost, E.A.K., 1985, Magmas and Magmatic Rocks: London & New York, Longman, v. 123, no. 1, 257 p.

Miri Beydokhti, R., Karimpour, M.H., Mazaheri, S.A., Santos, J.F., and Klötzlid, U., 2015, U–Pb zircon geochronology, Sr–Nd geochemistry, petrogenesis and tectonic setting of Mahoor granitoid rocks (Lut Block, Eastern Iran): Asian Earth Sciences, v. 111, p. 192–205.

Moghadam, H.S., Khademi, M., Hu, Z.C., Stern, R.J., Santos, J.F., and Wu, Y.B., 2015, Cadomian (Ediacaran–Cambrian) arc magmatism in the ChahJam–Biarjmand metamorphic complex (Iran): magmatism along the northern active margin of Gondwana: Gondwana Research, v. 27, p. 439–452.

Moghadam, H.S., Rossetti, F., Lucci, F., Chiaradia, M., Gerdes, A., Martinez, M.L., Ghorbani, G., and Nasrabady, M., 2016, The calc–alkaline and adakitic volcanism of the Sabzevar structural zone (NE Iran): implications for the Eocene magmatic flare–up in Central Iran: Lithos, v. 248–251, p. 517–535.

Moghadam, H.S., Li, X-H., Santos, J.F., Stern, R.J., Griffin, W.L., Ghorbani, G., and Sarebani, N., 2017, Neoproterozoic magmatic flare-up along the N. margin of Gondwana: the Taknar complex, NE Iran: Earth and Planetary Science Letters, v. 474, p. 83–96.

Moghadam, H.S., Griffin, W.L., Kirchenbaur, M., Garbe-Schönberg, D., Khedr, M.Z., Kimura, J.I., Stern, R.J., Ghorbani, G., Murphy, R., O'Reilly, S.Y., Arai, S., and Maghdour-Mashhour, R., 2018, Roll-Back, Extension and Mantle Upwelling Triggered Eocene Potassic Magmatism in NW Iran: Petrology, v. 59, no.7, p. 1417–1465.

Mohammadi, A., Burg, J.P., Bouilhol, P., and Ruh, J., 2016, U–Pb geochronology and geochemistry of Zahedan and Shah Kuh plutons, southeast Iran: Implication for closure of the South Sistan suture zone: Lithos, v. 248–251, p. 293–308.

Moradi Noghondar, M., Karimpour, M.H., Malekzadeh Shafaroudi, A., Farmer, G.L., and Stern, C., 2012, Geochemistry, zircon U-Pb geochronology and Rb-Sr & Sm-Nd isotopes of Najmabad monzonitic rocks south of Ghonabad: Iranian Journal of Petrology, no. 11, p. 77–95.

Nadermezerji, S., Karimpour, M.H., Malekzadeh Shafaroudi, A., Santos, J.F., Mathur, R., and Ribeiro, S., 2018, U–Pb geochronology, Sr–Nd isotopic compositions, geochemistry and petrogenesis of Shah Soltan Ali granitoids, Birjand, Eastern Iran: Chemie der Erde – Geochemistry, v. 78, p. 299–313.

Najafi, A., Karimpour, M.H., Ghaderi, M., Stern, C.R., and Farmer, J.L., 2014, Zircon U–Pb geochronology, isotope geochemistry of Rb–Sr and Sm–Nd and petrogenesis of granitoid intrusive rocks in Kajeh exploration area, northwest of Ferdows: evidence for Late Cretaceous magmatism in the Lut Block: Iranian Journal of Economic Geology, v. 6, no. 1, p.107–135.

Pang, K.-N., Chung, S.-L., Zarrinkoub, M.H., Khatib, M.M., Mohammadi, S.S., Chiu, H.-Y., Chu, C.-H., Lee, H.-Y., and Lo, C.-H., 2013, Eocene-Oligocene post-collisional magmatism in the Lut-Sistan region, eastern Iran: Magma genesis and tectonic implications: Lithos, v. 180–181, p. 234–251.

Pang, K.-N., Chung, S.-L., Zarrinkoub,M.H., Mohammadi, S.S., Yang, H.-M., Chu, C.-H., Lee, H.-Y., and Lo, C.-H., 2012, Age, geochemical characteristics and petrogenesis of Late Cenozoic intraplate alkali basalts in the Lut–Sistan region, eastern Iran: Chemical Geology, v. 306–307, p. 40–53.

Pearce, J.A., Harris, N.B.W., and Tindle, A.G., 1984, Trace element discrimination diagrams for the tectonic interpretation of granitic rocks: Petrology, v. 25, p. 956–983.

Pearce, J.A., and Peate, D.W., 1995, Tectonic implications of the composition of volcanic arc magmas: Annual Review of Earth and Plaentary Sciences, v. 23, p. 251–285.

Peccerillo, A., and Taylor, S.R., 1976, Geochemistry of Eocene calc-alkaline volcanic rocks from the Kastamonu area (Northern Turkey): Contributions to Mineralogy and Petrology, v. 58, no. 1, p. 63–81.

Rämö, O.T., Dall'Agnol, R., Macambira, M.J.B., Leite, A.A.S., and de Oliveira, D.C., 2002, 1.88 Ga oxidized A-type granites of the Rio Maria Region, Eastern Amazonian Craton, Brazil, positively anorogenic: Journal of Geology, v. 110, p. 603–610.

Richards, J.P., Spell, T., Rameh, E., Razique, A., and Fletcher, T., 2012, High Sr/Y reflect arc maturity, high magmatic water content, and porphyry Cu ± Mo ± Au potential: examples from the Tethyan arcs of central and eastern Iran western Pakistan: Economic Geology, v. 107, p. 295–332.

Rollinson, H.R., 1993, Using Geochemical Data: Evaluation, Presentation, Interpretation: New York, Longman Science and Technical, 352 p.

Rossetti, F., Nozaem, R., Lucci, F., Vignaroli, G., Gerdes, A., Nasrabadi, M., and Theye, T., 2015, Tectonic setting and geochronology of the Cadomian (Ediacaran-Cambrian) magmatism in Central Iran, Kuh-e-Sarhangi region (NW Lut Block): Asian Earth Sciences, v. 102, p. 24–44.

Rudnick, R.L., 1995, Making continental crust: Nature, v. 378, p. 571–578.

Saccani, E., Delavari, M., Beccaluva, L., and Amini, S., 2010, Petrological and geochemical constraints on the origin of the Nehbandan ophiolitic complex (eastern Iran): implication for the evolution of the Sistan Ocean: Lithos, v. 117, p. 209–228.

Salati, E., Karimpour, M.H., Malekzadeh Shafaroudi, A., Haidarian Shahri, M.R., Farmer, G.L., and Stern, C., 2013. Zircon dating (U-Pb), geochemistry of Sr-Nd isotopes and petrogenesis of oxidant granitoids in the Keybar Kuh area (southwest Khaf): Iranian Journal of Economic Geology, v. 4, no. 2, p. 281-301.

Salim, L., 2012, Geology, petrology and geochemistry of volcanic and sub volcanic rocks in Cheshme Khuri area (Northwest of Birjand) [MSc thesis]: Birjand, University of Birjand.

Samiee, S., Karimpour, M.H., Ghaderi, M., Haidarian Shahri, M.R., Klöetzli, U., and Santos, J.F., 2016, Petrogenesis of subvolcanic rocks from the Khunik prospecting area, south of Birjand, Iran: Geochemical, Sr–Nd isotopic and U–Pb zircon constraints: Asian Earth Sciences, v. 115, p. 170–182.

Schandl, E.S., and Gorton, M.P., 2002, Application of high field strength elements to discriminate tectonic settings in VMS environments: Economic Geology, v. 97, p. 629–642.

Schroder, J.W., 1944, Essai sur la structure de l'Iran: Ecologae Geologicae Helvetiae, v. 37, p. 37–81.

Shabanian, E., Acocella, V., Gioncada, A., Ghasemi, H., and Bellier, O., 2012, Structural control on volcanism in intraplate post collisional settings: Late Cenozoic to Quaternary examples of Iran and Eastern Turkey: Tectonics, v. 31, p. 1–25.

Stacey, J.S., and Kramers, J.D., 1975, Approximation of terrestrial lead isotope evolution by a two-stage model: Earth and Planetary Science Letters, v. 34, p. 207–226.

Steiger, R.H., and Jäger, E., 1977, Subcommision on geochronology: convention in the use of decay-constants in geo- and cosmochemistry: Earth and Planetary Science Letters, v. 36, p. 359–362.

Stocklin, J., and Nabavi, M.H., 1973, Tectonic map of Iran: Geological Survey of Iran.

Sun, S.S., and McDonough, W.F., 1989, Chemical and isotopic systematics of oceanic basalts: implications for mantle composition and processes: Geological Society of London Special Publication, v. 42, p. 313–345.

Tarkian, M., Lotfi, M., and Baumann, A., 1983, Tectonic, magmatism and the formation of mineral deposits in the central Lut, east Iran, Ministry of mines and metals: Geological Survey of Iran, Geodynamic Project (Geotraverse) in Iran, no, 51, p. 357–383.

Taylor, S.R., McLennan, S.M., 1985. The Continental Crust: Its Composition and Evolution: Oxford, Blackwell Scientific publications, 312 p.

Tirrul, R., Bell, I.R., Griffis, R.J., and Camp, V.E., 1983, The Sistan suture zone of eastern Iran. Geological Society of America Bulletin, v. 94, p. 134–150.

Verdel, C., Wernicke, B.P., Hassanzadeh, J., and Guest, B., 2011, A Paleogene extensional arc flare-up in Iran: Tectonics, v. 30, p. 1–20.

Vervoort, J.D., Patchett, P.J., Blichert- Toft, J., and Albarede, F., 1999, Relationship between Lu-Hf and Sm-Nd isotopic systems in the global sedimentary system: Earth and Planetary Science Letters, v. 168, p. 79–99.

Villa, I. M., De Bièvre, P., Holden, N. E., and Renne, P.R., 2015, IUPAC-IUGS recommendation on the half life of ^{87}Rb: Geochimica et Cosmochimica Acta, v. 164, p. 382–385.

Villagómez, D., Spikings, R., Magna, T., Kammer, A., Winkler, W., and Beltrán, A,. 2011, Geochronology, geochemistry and tectonic evolution of the Western and Central cordilleras of Colombia: Lithos, v. 125, p. 875–896.

Whalen, J.B., Currie, K.L., and Chappell, B.W., 1987, A-type granites: geochemical characteristics, discrimination and petrogenesis: Contributions to Mineralogy and Petrology, v. 95, p. 407–419.

Wilson, M., 1989, Igneous Petrogenesis A Global Tectonic Approach: New York, Harper Collins Academic, 466 p.

Winchester, J. A., and Floyd, P. A., 1977, Geochemical discrimination of different magma series and their differentiation protextures and setting of VMS mineralization in the Pilbara ducts using immobile elements: Chemistry Geology, v. 20, p. 325 – 344.

Zarrinkoub, M.H., Chung, S.-L., Chiu, H.-Y., Mohammadi, S., Khatib, M., and Lin, I.-J., 2010, Zircon U\Pb age and geochemical constraints from the northern Sistan suture zone on the Neotethyan magmatic and tectonic evolution in eastern Iran, in proceeding, Turkish Conference on Tectonic Crossroads: Evolving Orogens in Eurasia–Africa–Arabia, Oct. 4–8, Ankara, Turkey, p. 515–520.

Zarrinkoub, M.H., Pang, K.-N., Chung, S.-L., Khatib, M.M., Mohammadi, S.S., Chiu, H.-Y., and Lee, H.-Y., 2012, Zircon U\Pb age and geochemical constraints on the origin of the Birjand ophiolite, Sistan suture zone, eastern Iran: Lithos, v. 154, p. 392–405.

Zirjani Zadeh, S., 2015, Mineralization, geochemistry and petrogenesis of igneous rocks in northwest of Gonabad [Ph.D. Thesis]: Mashhad, Ferdowsi University of Mashhad, 412 p.

Appendix

Table 1. Whole-rock major and trace element compositions of volcanic and intrusive rocks of Khur area.

Sample	SH4	SH5	SH8	SH19	SH33	CH3	CH5	CH16	CH19
X	58˚23′31″	58˚23′33″	58˚22′54″	58˚23′32″	58˚21′10″	58˚25′10″	58˚25′25″	58˚ 24′ 21″	58˚24′ 30″
Y	33˚3′ 12″	33˚ 3′ 1″	33˚4′ 5″	33˚2′ 3″	33˚2′ 53″	33˚9′ 19.3″	33˚9′ 18″	33˚ 11′ 52″	33˚ 13′ 13″
Type	Ta	Ta	Ta	Ta	Ta	D	D	Ba	A
Wt.%									
SiO_2	56.52	55.76	57.63	60.17	55.47	63.11	63.73	55.13	60.81
TiO_2	1.64	1.68	1.57	1.08	1.76	0.51	0.45	0.96	0.67
Al_2O_3	16.1	16.28	16.06	15.59	16.25	17.09	16.98	16.75	15.34
TFeO	7.56	7.76	6.35	6.06	7.05	4.34	3.9	7.5	5.37
MnO	0.13	0.16	0.12	0.11	0.15	0.08	0.05	0.15	0.1
MgO	2.41	2.09	2.21	1.88	2.38	1.23	1.64	4.3	3.49
CaO	5.85	6.03	5.59	4.95	6.14	3.88	3.31	7.29	4.79
Na_2O	3.2	3.18	3.31	3.24	3.05	2.98	2.82	3.06	3.42
K_2O	3.47	3.68	3.47	3.84	3.68	2.92	3.01	2.46	3.13
P_2O_5	0.98	1	1.01	0.62	0.92	0.21	0.18	0.32	0.16
LOI	1.05	1.26	1.73	1.55	2.11	3	3.33	0.96	1.85
Total	98.91	98.88	99.05	99.09	98.96	99.35	99.4	98.88	99.13
ppm									
Ba	515	514	490	581	515	467	469	655	867
Be	4	3	4	4	3	2	3	1	<1
Co	18.3	18.9	17.1	12.5	17.0	5.5	5.1	16.8	27.5

Cs	4.8	7.3	5.5	6.4	3.8	4.1	2.8	1.9	2.1
Ga	18.5	18.6	17.7	18.5	19.0	17.1	16.1	15.5	16.5
Hf	9.1	9.2	9.0	8.5	9.2	4.1	4.1	3.3	3.5
Nb	15.4	15.1	15.2	14.3	16.6	7.0	7.0	8.6	7.1
Rb	158.6	179.7	156.1	169.4	150.0	96.6	98.5	74.8	69.4
Sn	3	3	3	2	3	1	<1	1	<1
Sr	401.1	419.6	388.6	400.6	408.6	368.7	338.9	613.6	1135.0
Ta	0.9	1.2	1.1	0.9	1.1	0.4	0.5	0.5	0.6
Th	19.9	20.9	20.2	18.4	20.5	9.7	9.7	7.4	9.8
U	4.9	4.9	5.0	4.6	4.8	2.4	2.7	3.6	2.5
V	176	179	162	99	176	42	66	114	250
W	1.7	2.2	2.6	2.5	2.3	1.4	1.4	1.4	0.8
Zr	385.9	398.5	389.9	360.0	400.2	160.9	156.7	130.5	123.1
Y	45.3	49.5	43.7	39.1	48.1	10.7	10.8	13.0	20.4
La	52.6	52.5	52.6	46.2	54.0	27.1	26.9	21.7	33.9
Ce	105.3	110.7	106.8	94.0	109.8	55.8	55.2	39.4	69.3
Pr	12.50	13.00	12.44	10.74	13.00	6.03	5.99	4.25	7.83
Nd	48.0	52.6	50.1	41.7	52.8	22.5	23.5	15.9	31.7
Sm	9.81	10.62	9.92	8.15	10.34	4.21	4.20	2.84	6.32
Eu	2.23	2.34	2.17	1.94	2.25	1.04	1.00	0.80	1.55
Gd	9.50	9.59	9.01	7.60	9.55	3.33	3.21	2.61	5.12
Tb	1.53	1.53	1.43	1.24	1.51	0.47	0.46	0.40	0.72
Dy	8.60	8.75	8.37	7.26	8.62	2.31	2.50	2.21	4.13
Er	5.10	5.29	4.82	4.48	5.10	1.10	1.21	1.37	2.20
Tm	0.76	0.79	0.71	0.64	0.75	0.14	0.16	0.18	0.34
Yb	5.02	5.08	4.40	4.21	4.96	0.95	1.07	1.40	2.36
Lu	0.74	0.79	0.70	0.67	0.74	0.15	0.14	0.21	0.34
Ratios									
*Eu/Eu	0.706	0.709	0.702	0.754	0.692	0.849	0.833	0.898	0.833
$(La/Yb)_N$	7.064	6.968	8.06	7.399	7.34	19.232	16.949	10.45	9.684

Table 1 *(continued)*

Sample	CH31	SH6	SH11	SH35	SH36	SH67	H14	H10

X	58° 24′ 8″	58°22′15″	58°22′18″	58°23′7″	58°22′2″	58°24′1″	58°26′39″	58°26′41″
Y	33° 11′ 41″	33°3′ 55″	33°3′ 27″	33°2′9″	33°2′6″	33°2′7″	33°7′25″	33°7′3″
Type	A	Mz	Mz	Mz	Mz	Mz	Di	Di
Wt.%								
SiO_2	59.18	55.12	55.91	56.92	56.05	56.28	62.18	58.02
TiO_2	0.84	1.7	1.6	1.35	1.45	1.58	0.76	0.96
Al_2O_3	16.05	16.36	17.11	17.35	16.44	16.53	15.77	16.21
TFeO	6.59	8.34	7.91	7.13	7.46	7.83	5.47	6.46
MnO	0.14	0.14	0.12	0.1	0.09	0.1	0.15	0.13
MgO	3.94	2.63	2.37	2.2	2.54	2.46	1.97	3.36
CaO	6.17	5.94	6.12	5.84	6.19	5.90	5.65	6.97
Na_2O	3.05	3.18	3.35	3.42	3.26	3.36	2.99	3.64
K_2O	2.59	3.79	3.68	3.6	3.61	3.70	2.9	1.19
P_2O_5	0.19	0.97	0.91	0.81	0.92	0.90	0.21	0.38
LOI	0.28	1.59	0.85	1.05	1.76	1.23	1.76	1.76
Total	99.02	99.76	99.93	99.77	99.77	99.87	99.81	99.81
ppm								
Ba	581	507	487	436	409	445	276	330
Be	<1	3	5	7	1	6	<1	3
Co	23.2	18.1	18.6	15.0	16.9	17.3	16.0	23.6
Cs	2.4	4.5	3.7	4.1	3.1	4.2	15.0	19.6
Ga	16.3	18.8	18.65	17.9	18.5	18.23	15.0	14.2
Hf	3.5	9.1	8.6	7.6	7.0	7.9	3.8	4.1
Nb	7.9	16.1	13.2	12.0	12.3	14.6	6.1	7.2
Rb	70.5	155.9	136.7	125.2	121.7	149.8	66.7	50.3
Sn	1	2	2	2	2	2	2	1
Sr	699.4	389.8	426.7	446.2	441.8	435.2	393.7	478.6
Ta	0.6	1.0	0.9	0.8	0.7	0.7	0.4	0.5
Th	6.9	19.6	18.5	15.0	15.1	17.4	8.3	8.5
U	2.1	4.9	3.7	3.5	3.4	4.2	1.9	1.9

V	160	166	137	130	143	159	112	163
W	0.7	2.1	2/0	1.7	1.5	1.9	1.1	1.5
Zr	134.6	381.3	325.7	313.9	305.3	339.5	156.3	178.8
Y	16.3	42.9	38.9	36.5	34.4	41.3	16.3	19.4
La	21.3	52.7	50.4	41.6	40.6	45.7	20.4	24.1
Ce	43.9	104.6	98.5	84.5	82.2	87.1	37.7	48.0
Pr	4.91	12.46	10.84	9.88	9.47	9.59	4.35	5.33
Nd	19.3	48.0	37.4	38.3	36.7	38.7	17.0	20.8
Sm	3.83	9.63	9.57	7.98	7.52	8.63	3.21	4.27
Eu	1.09	2.13	2.10	1.90	1.87	1.95	1.04	1.22
Gd	3.66	8.92	8.67	7.64	7.48	7.87	3.14	4.03
Tb	0.56	1.47	1.36	1.15	1.09	1.29	0.48	0.67
Dy	3.36	7.77	6.81	6.74	6.66	7.39	2.64	3.79
Er	2.05	4.75	4.16	4.05	3.46	4.37	1.55	2.18
Tm	0.30	0.67	0.56	0.58	0.52	0.63	0.23	0.34
Yb	2.04	4.59	4.25	3.61	3.56	3.78	1.62	2.17
Lu	0.30	0.70	0.65	0.58	0.55	0.59	0.24	0.35
Ratios								
*Eu/Eu	0.89	0.703	0.709	0.744	0.762	0.735	1.002	0.899
$(La/Yb)_N$	7.039	7.741	7.753	7.769	7.689	7.675	8.49	7.488

Table 1 *(continued)*

Sample	D4	D5	D9	D16	D23	D24	D32	D33	D69
X	58°29′15″	58°29′5″	58°29′36″	58°28′46″	58°29′40″	58°29′29″	58°29′35″	58°29′46″	58°28′56″
Y	33°4′34″	33°2′55″	33°3′7″	33°3′20″	33°3′31″	33°3′36″	33°2′39″	33°4′18″	33°5′16″
Petrography	Di	Gr	Gd	Gd	G	Gd	Di	Gr	Gd
Wt. %									
SiO_2	58.42	61.82	54.23	54.6	49.68	53.77	64.95	67.69	54.39
TiO_2	0.99	0.65	1.02	1.01	1.02	0.93	0.64	0.34	1.14
Al_2O_3	16.1	15.28	15.62	16.99	15.32	17.9	15.18	15.3	16.26
FeOt	7.09	5	7.85	7.16	9.4	8	5.33	3.4	8.76

MnO	0.13	0.08	0.15	0.12	0.15	0.15	0.09	0.09	0.14
MgO	3.32	3.2	4.96	4.77	8.35	4.11	1.72	0.95	4.49
CaO	6.04	4.85	8.55	7.81	9.48	9.17	4.85	3.92	7.55
Na_2O	2.5	3.23	2.41	3.16	2.08	2.84	3.02	3.39	2.79
K_2O	3.18	3.68	2.56	1.84	1.6	2.12	2.95	3.08	2.34
P_2O_5	0.33	0.21	0.32	0.3	0.36	0.43	0.33	0.19	0.34
LOI	1.7	1.83	2.15	2.05	2.38	0.4	0.75	1.49	1.59
Total	99.8	99.83	99.82	99.81	99.82	99.82	99.81	99.84	99.79
ppm									
Ba	311	347	421	306	250	325	511	509	391
Be	<1	<1	<1	<1	2	2	1	<1	1
Co	21.6	10.6	27.8	22.9	32.5	25.5	7.2	3.3	27.4
Cs	12.7	1.3	2.3	1.3	0.6	4.3	1.8	2.6	3.7
Ga	15.2	14.1	16.1	15.2	14.3	15.8	13.5	13.0	16.4
Hf	4.4	4.2	3.3	3.5	2.9	3.0	4.1	3.8	5.2
Nb	7.6	5.6	5.1	8.3	3.9	4.4	8.6	7.0	9.7
Rb	66.6	42.6	71.2	52.8	27.8	52.0	85.2	108.6	56.4
Sn	1	2	1	1	<1	<1	<1	1	2
Sr	466.6	410.3	552.4	450.6	472.0	533.2	417.6	425.7	519.4
Ta	0.6	0.6	0.3	0.7	0.2	0.3	0.6	0.6	0.6
Th	9.1	9.9	8.0	6.7	4.5	6.2	7.2	10.4	12.1
U	1.9	2.7	1.9	1.7	1.0	1.4	2.0	3.0	3.0
V	172	110	246	240	227	261	85	34	230
W	0.9	1.1	1.0	0.5	<0.5	0.8	2.7	1.3	1.7
Zr	184.3	165.7	129.3	157.1	109.0	114.9	161.5	167.4	195.2
Y	18.7	14.8	22.2	19.2	20.0	20.4	19.1	14.0	26.7
La	25.1	19.0	22.7	19.6	16.9	17.6	23.5	24.7	29.9
Ce	49.8	38.4	49.7	39.3	32.5	35.5	46.6	44.3	60.1
Pr	5.50	4.15	5.89	4.52	3.99	4.22	5.27	4.88	7.07
Nd	22.1	16.3	24.6	17.7	16.9	19.3	20.6	18.3	28.7
Sm	4.43	2.97	5.73	3.99	3.61	3.76	3.84	2.96	5.60
Eu	1.20	0.82	1.48	1.05	1.14	1.23	1.12	0.84	1.38
Gd	3.98	2.87	4.71	3.80	3.86	4.09	3.83	2.59	5.91
Tb	0.65	0.47	0.79	0.66	0.63	0.64	0.61	0.40	0.86

Dy	3.73	2.77	4.11	4.02	3.75	3.85	3.52	2.52	5.22
Er	2.22	1.59	2.46	2.29	2.23	2.31	2.23	1.60	2.90
Tm	0.33	0.24	0.37	0.37	0.32	0.34	0.34	0.24	0.44
Yb	2.06	1.48	2.26	2.29	2.12	2.14	2.20	1.91	2.83
Lu	0.33	0.24	0.34	0.35	0.33	0.31	0.35	0.29	0.40
Ratios									
*Eu/Eu	0.874	0.859	0.871	0.825	0.934	0.959	0.893	0.928	0.733
$(La/Yb)_N$	8.215	8.655	6.772	5.77	5.374	5.545	7.202	8.719	7.123

Abbreviations: R: Rhyodacite, D: Dacite, A: Andesite, Ta: Trachyandesite, Ba: Basaltic andesite, G: Gabbro, Gd: Gabbrodiorite, Mz: Monzonite, Di: Diorite, Gr: Granodiorite, LOI: Loss on Ignition.

Table 2. Rb–Sr and Sm–Nd isotopic data of eleven whole-rock samples from the Khur area.

Sampl	Sr	Rb	$^{87}Rb/^{8}$	Error	$^{87}Sr/^{86}S$	Error	$(^{87}Sr/^{86}S$	Nd	Sm	$^{147}Sm/^{1}$	Error		Error	εNdi
D4	467	67	0.415	0.012	0.70510	0.00002	0.70484	22.1	4.4	0.120	0.00	0.512774	0.0000	+3.1
D23	472	27	0.170	0.005	0.70485	0.00002	0.70475	16.9	3.6	0.129	0.00	0.512733	0.0000	+2.2
D24	533	52	0.282	0.008	0.70492	0.00001	0.70476	19.3	3.8	0.118	0.00	0.512702	0.0000	+1.6
D32	418	85	0.588	0.017	0.70512	0.00002	0.70479	20.6	3.8	0.112	0.00	0.512773	0.0000	+3.1
D33	426	109	0.738	0.021	0.70540	0.00001	0.70498	18.3	3.0	0.098	0.00	0.512631	0.0000	+0.3
SH6	390	156	1.156	0.033	0.70545	0.00002	0.70479	-	-	-	-	-	-	-
SH35	446	125	0.812	0.023	0.70524	0.00002	0.70478	38.3	8.0	0.126	0.00	0.512782	0.0000	+3.1
CH16	113	69	0.177	0.005	0.70506	0.00002	0.70496	31.7	6.3	0.121	0.00	0.512656	0.0000	+0.7
SH4	420	180	1.238	0.035	0.70540	0.00002	0.70469	52.6	10.	0.122	0.00	0.512772	0.0000	+3.0
SH5	401	159	1.144	0.032	0.70563	0.00002	0.70498	48.0	9.8	0.124	0.00	0.512759	0.0000	+2.7
SH19	409	150	1.061	0.030	0.70546	0.00002	0.70485	52.8	10.	0.118	0.00	0.512710	0.0000	+1.8

Note: ^{87}Rb decay λ = 1.3972 × 10^{-11} a^{-1} (Villa et al., 2015); ^{147}Sm decay λ = 6.54 × 10^{-12} a^{-1} (Steiger and Jager, 1977); The ^{143}Nd/^{144}Nd and ^{147}Sm/^{144}Nd ratios of chondrite at present day are 0.512638 and 0.1967, respectively (Jacobsen and Wasserburg, 1980).

Table 3. Results of U–Pb–Th the laser-ablation multicollector ICP mass spectrometry analysis of zircon from dike of diorite and monzonite.

Spot	U (ppm)	^{206}Pb /^{204}Pb	U/Th	^{206}Pb/ ^{207}Pb	± (%)	^{207}Pb/ ^{235}U	± (%)	^{206}Pb/ ^{238}U	± (%)	^{206}Pb/ ^{238}U (Ma)	± (Ma)
D45- 36	300	19712	1.9	20.2087	2.3	0.0471	3.6	0.0069	2.7	44.4	1.2
D45- 37	156	3690	1.6	21.3277	2.8	0.0448	4.0	0.0069	2.8	44.5	1.2
D45- 38	273	2416	2.0	22.6357	2.9	0.0425	4.0	0.0070	2.7	44.8	1.2
D45- 39	212	4213	1.4	23.2514	3.0	0.0402	4.1	0.0068	2.9	43.6	1.3
D45- 40	571	2676	2.0	22.2960	1.6	0.0429	3.3	0.0069	2.8	44.6	1.3
D45- 41	69	1584	1.4	25.0079	8.6	0.0386	9.1	0.0070	3.2	45.0	1.4
D45- 42	452	6224	2.2	21.1039	2.0	0.0462	3.3	0.0071	2.6	45.5	1.2
D45- 43	259	1964	1.5	25.1790	3.2	0.0384	4.4	0.0070	2.9	45.1	1.3
D45- 44	633	20274	1.7	21.0806	1.5	0.0477	3.1	0.0073	2.7	46.8	1.2
D45- 45	470	3055	2.0	13.2226	5.6	0.0753	6.9	0.0072	4.0	46.4	1.9
D45- 46	472	11564	1.5	20.4629	1.8	0.0465	3.4	0.0069	2.9	44.4	1.3
D45- 47	1130	18579	1.1	21.2615	1.4	0.0441	6.3	0.0068	6.1	43.7	2.7
D45- 48	933	61129	1.7	18.6315	1.6	0.0525	3.2	0.0071	2.8	45.6	1.3
Monzonite											
SH6-1	226	1930	1.4	15.3936	5.1	0.0545	5.1	0.0061	3.8	39.1	1.3
SH6-2	265	36627	1.2	18.5838	2.4	0.0464	3.9	0.0064	3.0	42.6	1.3
SH6-3	187	21935	1.0	21.6323	3.1	0.0409	3.5	0.0064	3.2	41.1	1.4
SH6-4	315	60035	1.4	20.0623	2.1	0.0444	2.3	0.0064	2.5	41.4	1.3
SH6-5	276	23145	1.0	21.7221	3.2	0.0408	3.4	0.0063	3.1	41.2	1.5

SH6-6	259	37891	1.2	21.5326	3.7	0.0401	3.1	0.0063	2.9	40.3	2.2
SH6-7	463	29863	1.0	19.8436	3/8	0.0415	3.2	0/0063	2.9	39.3	0.9
SH6-8	258	95245	0.9	21.7223	2.4	0.0410	3.4	0.0064	4.1	41.3	2.0
SH6-9	465	128786	1.0	20.3438	2.4	0.0420	3.8	0.0062	3.7	39.6	2.1
SH6-10	297	1367	0.9	17.8336	3.6	0.0424	2.8	0.0063	3/6	40.3	4.1
SH6-11	1678	12571	0.7	20.2623	2.3	0.0453	3.4	0.0066	2.7	42.6	1.5
SH6-12	783	203467	3.7	17.6236	2.1	0.6729	1.7	0.0864	3.6	527.4	12.5
SH6-13	345	25612	5.9	17.1456	0.8	0.6918	1.1	0.0849	3.1	530.2	14.3
SH6-14	287	115431	3.6	17.6323	1.2	0.7387	1.3	0.0887	2.2	553.9	14.1
SH6-15	253	12463	6.8	17.3923	1.1	0.7412	1.2	0.0925	2.3	572.6	14.0
SH6-16	367	63467	1.8	17.0063	1.2	0.7213	1.4	0.0886	3.2	546.3	14.9
SH6-17	451	29345	1.4	19.3263	1.3	0.7132	1.5	0.0880	1.1	543.1	4.9
SH6-18	542	29763	2.4	17.0345	2.1	0.7161	3.1	0/0883	3.7	545.9	17.1
SH6-19	678	56934	1.5	17.0698	0.9	0.7056	1.4	0/0873	1.1	541.2	5.7
SH6-20	467	43754	2.3	17.0389	1.1	0.7067	1.5	0/0874	1.3	539.2	7.1

Table 4. U–Pb data obtained by ID-TIMS from zircon in dike of granodiorite (sample CH4).

zircon type	U (ppm)	Th/U	$^{206}Pb/^{204}Pb$	$^{207}Pb/^{235}U$	2 sigma	$^{206}Pb/^{238}U$	2 sigma	Rho	$^{207}Pb/^{206}Pb$	2 sigma	$^{206}Pb/^{238}U$ [Ma]	2 sigma [Ma]	$^{207}Pb/^{235}U$ [Ma]	2 sigma [Ma]	Disc. (%)	zircon type	U (ppm)
tip	124	0.20	60	0.03876	0.00481	0.00635	0.00007	0.36	0.04427	0.00533	40.8	0.5	38.6	4.7	0.0	176.4	2.3
short prisms	219	0.53	54	0.11810	0.00863	0.01364	0.00015	0.08	0.06279	0.00458	87.3	1.0	113.3	7.8	701.1	148.2	88.1
short prisms	131	0.39	341	0.07960	0.00111	0.01130	0.00004	0.39	0.05109	0.00067	72.4	0.2	77.8	1.0	244.7	29.8	70.8

short prisms	205	0.32	42	0.29333	0.01921	0.02002	0.00032	0.13	0.10628	0.00695	127.8	2.1	261.2	15.0	1736.5	115.4	93.5
short prisms	148	0.49	3114	0.77831	0.00208	0.05159	0.00011	0.86	0.10941	0.00015	324.3	0.7	584.5	1.2	1789.6	2.5	83.9
tip	70	0.20	134	0.08684	0.00260	0.01104	0.00006	0.28	0.05704	0.00165	70.8	0.4	84.6	2.4	493.2	62.6	86.1
tip	352	0.27	971	0.38102	0.00220	0.05097	0.00014	0.57	0.05422	0.00027	320.5	0.9	327.8	1.7	380.1	11.2	16.1

Explanation: Rho is the correlation between the $^{206}Pb/^{238}U$ and $^{207}Pb/^{235}U$ ratios; 2 sigma uncertainties are calculated by propagating the uncertainties from measurement, fractionation, blank correction and common Pb correction.

Figure captions

Figure 1- Simplified geological map of Iran showing the distribution of Eocene magmatic rocks and Mesozoic ophiolites in Iran (modified after Shafaii Moghadam et al., 2015).

Figure 2- Major Tertiary mineralization occurrences associated with the Late Cretaceous-Oligocene I-type granitoids within the Lut Block (Mahdavi et al., 2016; Arjmandzadeh and Santos, 2014; Arjmandzadeh et al. 2011; Malekzadeh Shafaroudi et al., 2012, 2015; Nadermezerji et al., 2018; Samiee et al., 2015; Miri Beydokhti et al., 2015; Abdi and Karimpour, 2013; Hosseinkhani et al., 2017; Najafi et al., 2014; Zirjani Zadeh, 2015; Salati et al., 2013; Moradi et al., 2012, Jung et al, 1983; Javidi Moghaddam et al., 2019).

Figure 3- Simplified geological map of the Khur area (modified after Sarghanj 1/100000 map).

Figure 4- Field photographs of the Khur magmatic rocks. (a) Outcrops of rhyolitic and andesitic tuff breccias, (b) outcrops of dikes in the southern parts of the Khur area, (c) granodiorite dikes crosscut andesitic tuff breccias, (d) outcrops of diorite dikes, (e) gabbroic dikes crosscut granodiorite dikes.

Figure 5- (a) Classification diagrams for the geochemical classification of the Khur samples. (a) Na_2O+ K_2O *vs* SiO_2 (TAS) diagram (Middlemost, 1985), (b) Zr/TiO_2 *vs* SiO_2 (Winchester and Floyd, 1977), (c) K_2O *vs* SiO_2 diagram (Peccerillo and Taylor, 1976), (d) $Al_2O_3/Na_2O + K_2O$

(molar) *vs* $Al_2O_3/(CaO + K_2O + Na_2O)$ diagram (molar) (Maniar and Piccoli, 1989). The field boundaries between S-type and I-type granite are from Chappell and White (1992).

Figure 6- (a) $FeO_t/(FeO_t + MgO)$ *vs* SiO_2 diagram for the classification of the Khur felsic rocks The ferroan-magnesian boundary is from Frost et al. (2001). (b) Modified alkali-lime index (MALI) ($Na_2O + K_2O/CaO$) *vs* SiO_2. The alkalic, alkali-calcic, calc-alkalic, and calcic boundaries are after Frost et al. (2001).

Figure 7- primitive-mantle-normalized trace elements (normalizing values after Sun and McDonough (1989)) and chondrite-normalized rare earth elements (normalizing values after Boynton (1984)) patterns for the Khur dikes (a–b), the monzonite (c–d), the volcanic rocks (e–f) and trachyandesite rocks (g–h).

Figure 8- Diagram of εNd(i) vs. $(^{87}Sr/^{86}Sr)i$ for Khur rocks. Reference data sources: upper continental crust (Taylor and McLennan, 1985); lower continental crust (Rollinson, 1993; Rudnick, 1995), MORB (Rollinson, 1993; Sun and McDonough, 1989), DM (McCulloch and Bennett, 1994), OIB (Vervoort et al., 1999) and mantle array (Wilson, 1989; Gill, 1981; McCulloch et al., 1994). MORB: Mid-ocean ridge basalts; DM: Depleted mantle; OIB: Ocean-island basalts. Data for Late Cretaceous-Oligocene I-type granitoids from Arjmandzadeh and Santos, 2014; Arjmandzadeh et al. 2011; Malekzadeh Shafaroudi et al., 2012, 2015; Nadermezerji et al., 2018; Samiee et al., 2015; Miri Beydokhti et al., 2015; Abdi and Karimpour, 2013; Hosseinkhani et al., 2017; Najafi et al., 2014; Zirjani Zadeh, 2015; Salati et al., 2013; Moradi et al., 2012; Jung et al, 1983.

Figure 9- U–Pb inverse concordia diagrams (a, c) and average age plots (b,d) for the diorite dike (D33), above, and the monzonite (SH6), below.

Figure 10- U–Pb Concordia diagrams for zircon in the granodiorite dike (D4). Inset shows some typical zircon grains.

Figure 11- (a) Th/Yb vs. Ta/Yb (Pearce and Peate, 1995) and (b) Th/Nb vs. Ba/Nb (Ersoy et al., 2010) diagrams for the Khur rocks.

Figure 12- Tectonomagmatic discrimination diagram for the Khur rocks (a) Ta vs. Th (Schandl and Gorton, 2002), (b) Nb+Y vs. Rb and (b) Y vs. Nb (Pearce et al., 1984). WPG, within plate granites; VAG, volcanic arc granites; ORG, ocean ridge granites; syn-COLG, syncollisional granites.

Figure 13- (a) Yb, (b) Nb, (d) Zr, and (e) Ce vs. 10,000 Ga/Al discrimination diagrams for Khur rocks (Whalen et al., 1987).

Figure 14- Paleogeographic reconstructions of the Central-East Iranian Microcontinent (CEIM) (a) 90 Ma (Mattei et al., 2014) and (b) now. Y = Yazd; T = Tabas; L = Lut; A = Alborz; SCB = Southern Caspian Basin; CA = Central Afghanistan.

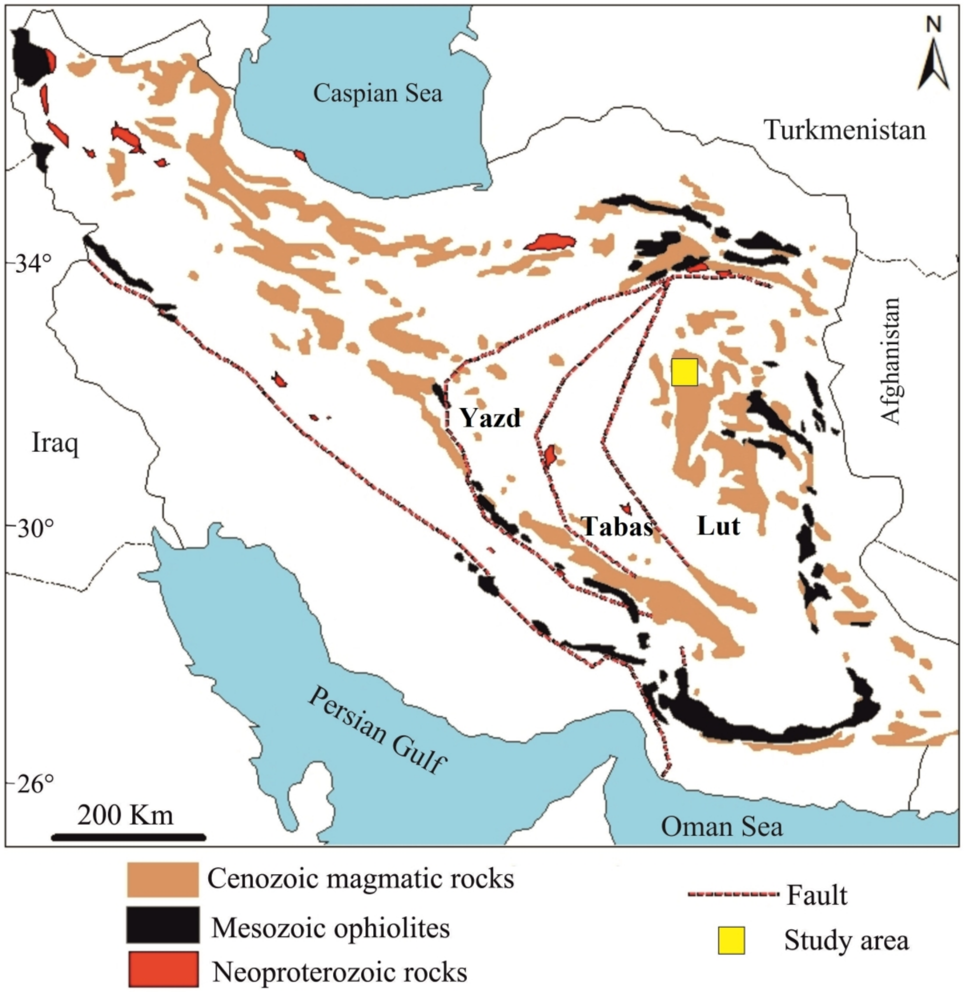

Fig. 1

214x219mm (300 x 300 DPI)

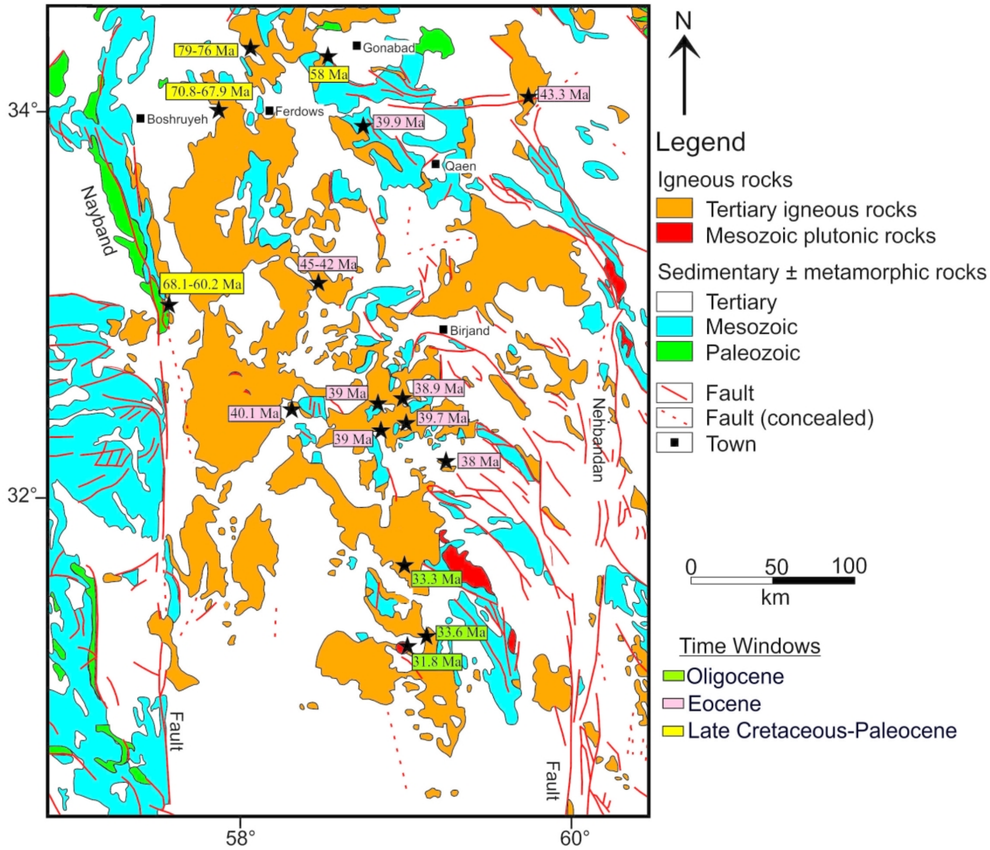

Fig. 2

195x166mm (300 x 300 DPI)

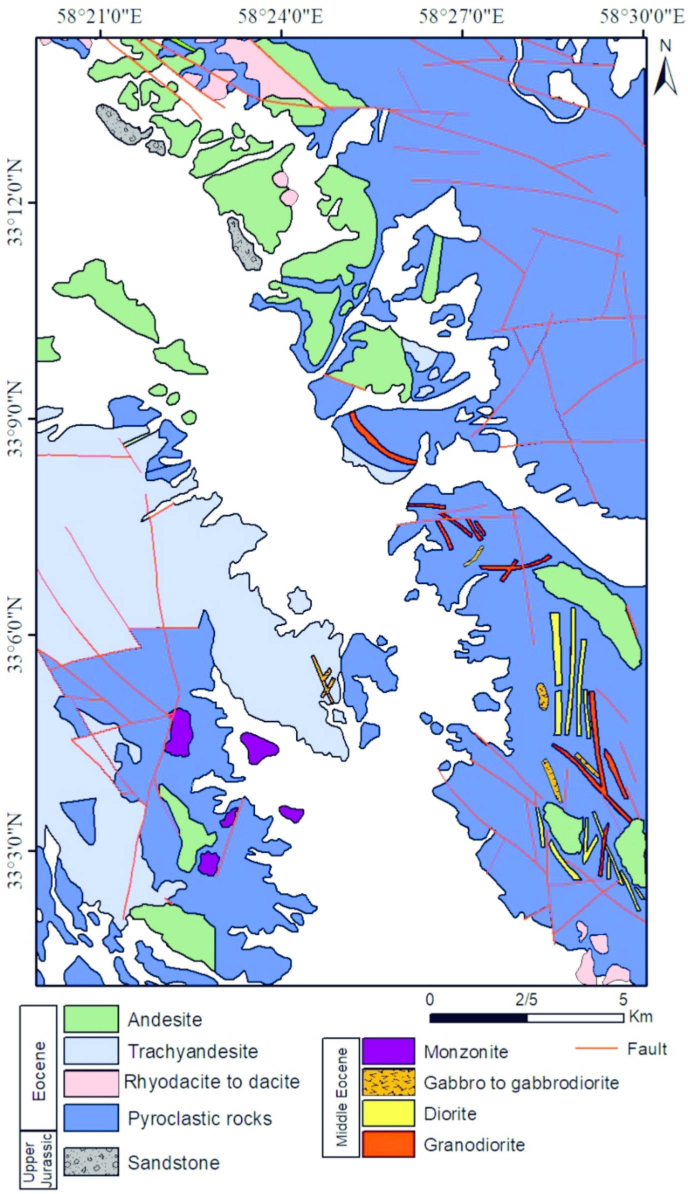

Fig. 3

165x280mm (300 x 300 DPI)

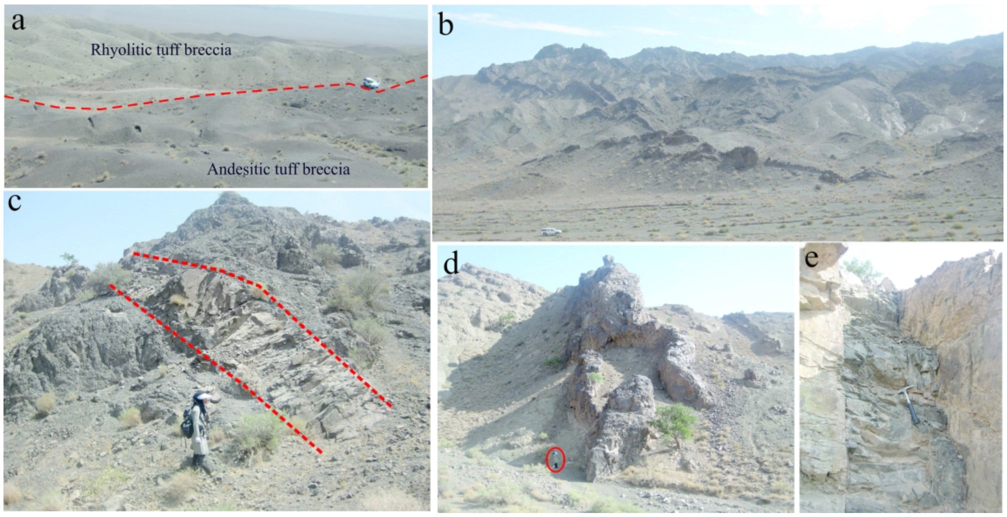

Fig. 4

423x215mm (300 x 300 DPI)

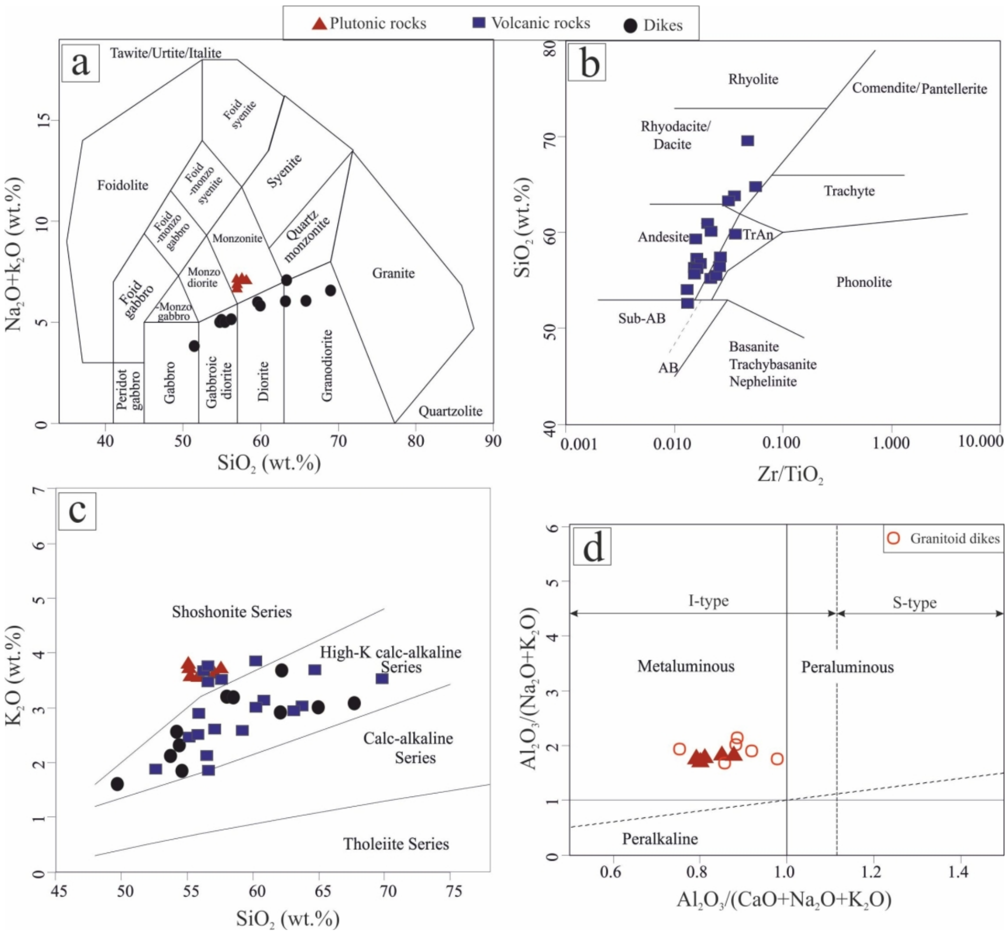

Fig. 5

186x172mm (300 x 300 DPI)

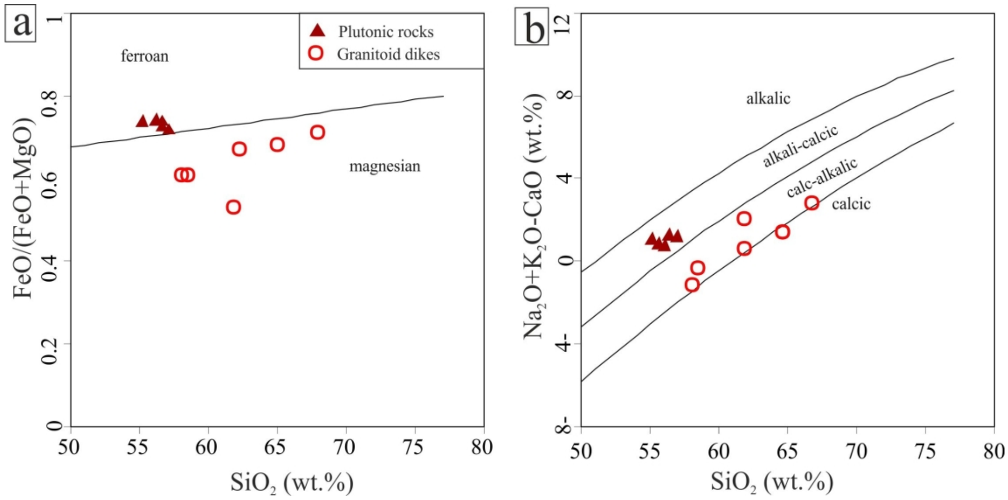

Fig. 6

191x94mm (300 x 300 DPI)

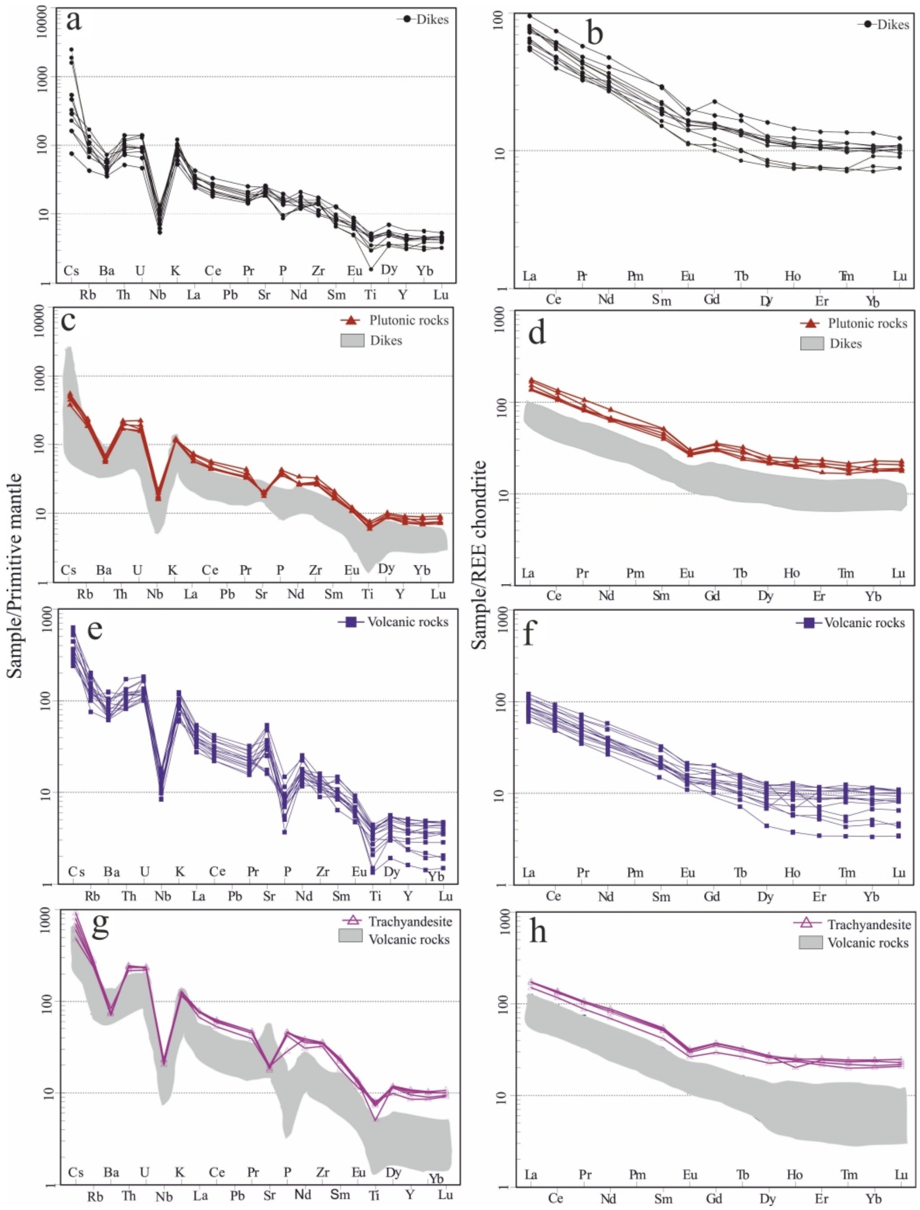

Fig. 7

321x423mm (300 x 300 DPI)

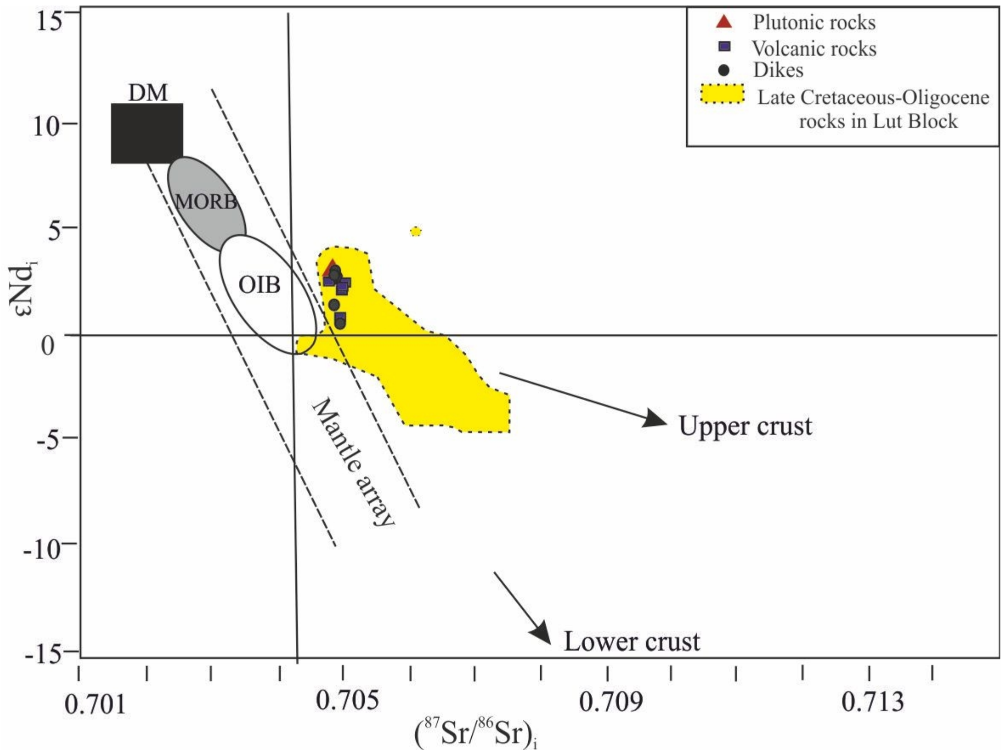

Fig. 8

99x74mm (300 x 300 DPI)

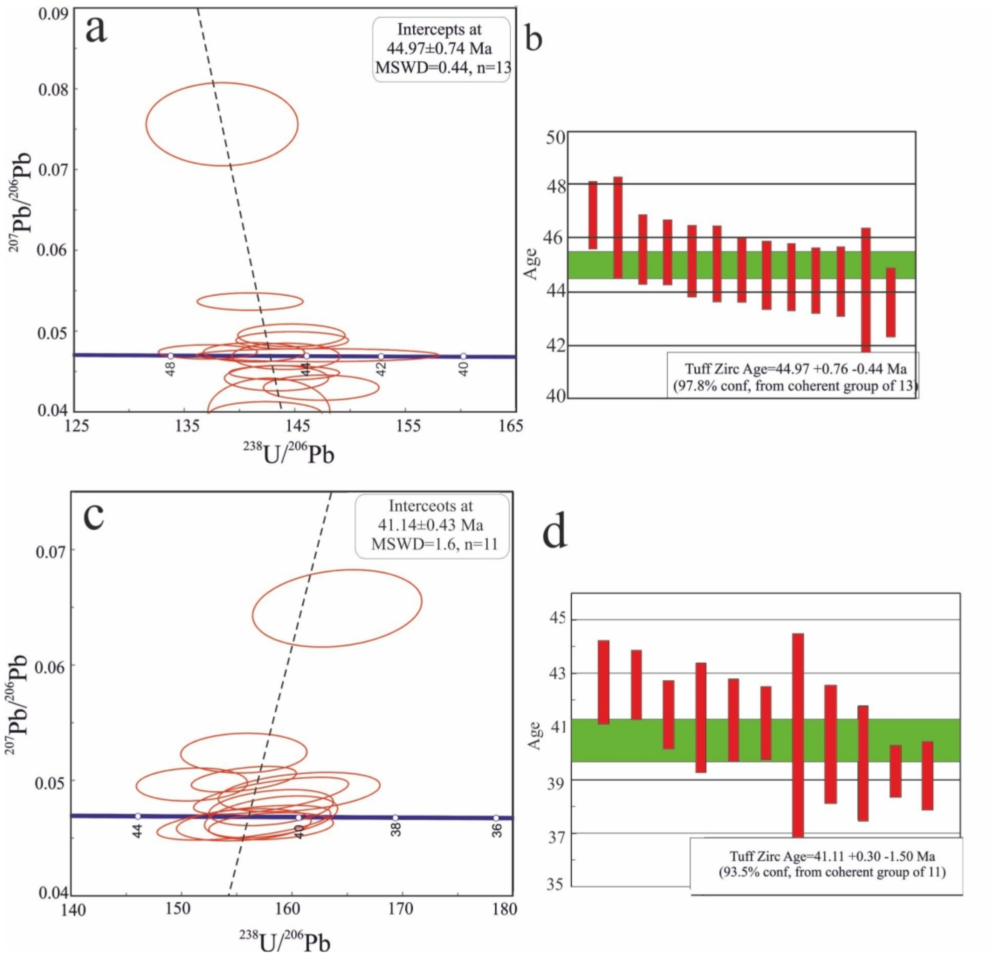

Fig. 9

165x156mm (300 x 300 DPI)

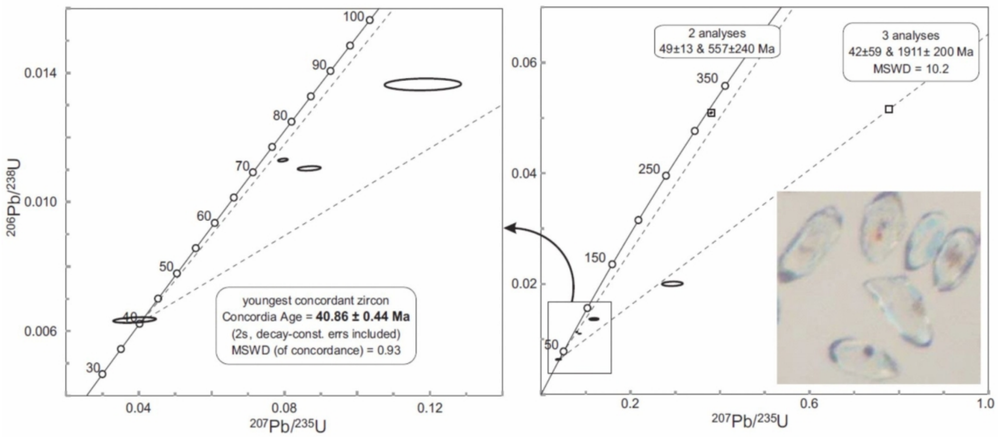

Fig. 10

165x74mm (300 x 300 DPI)

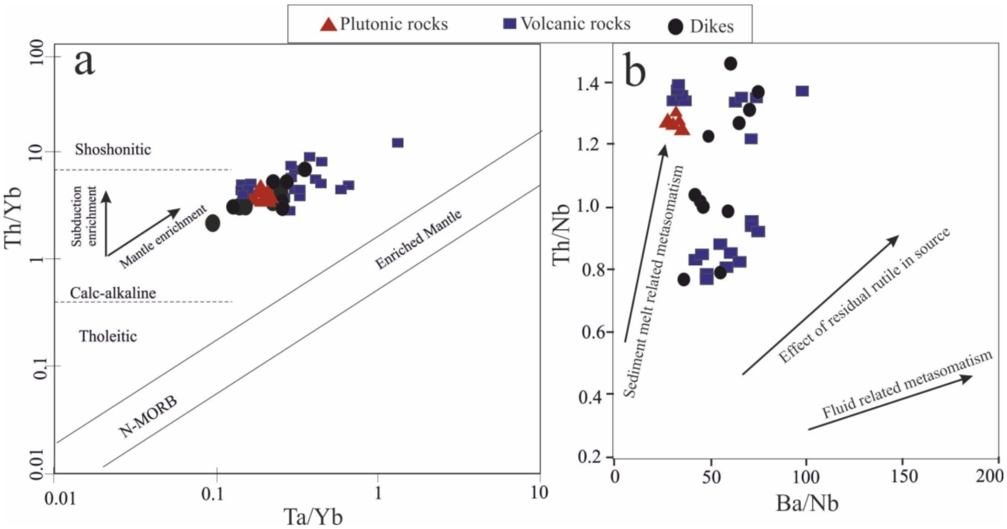

Fig. 11

186x97mm (300 x 300 DPI)

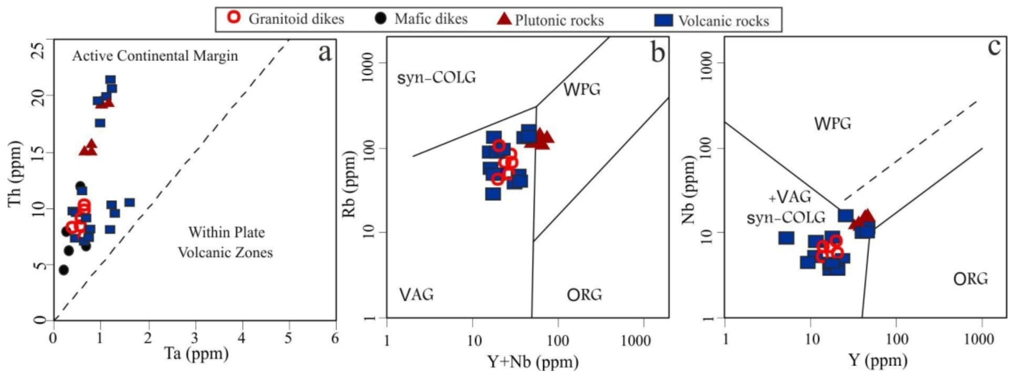

Fig. 12

160x59mm (300 x 300 DPI)

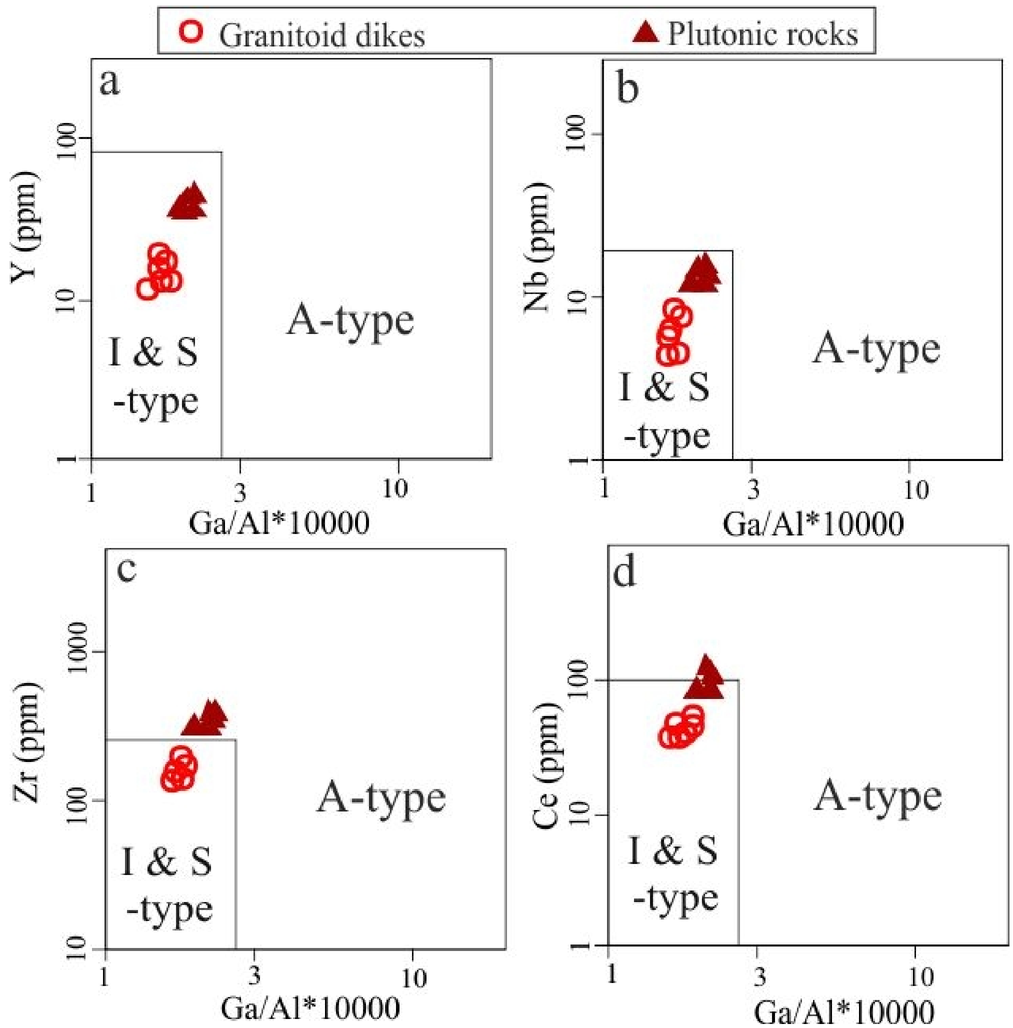

Fig. 13

53x54mm (300 x 300 DPI)

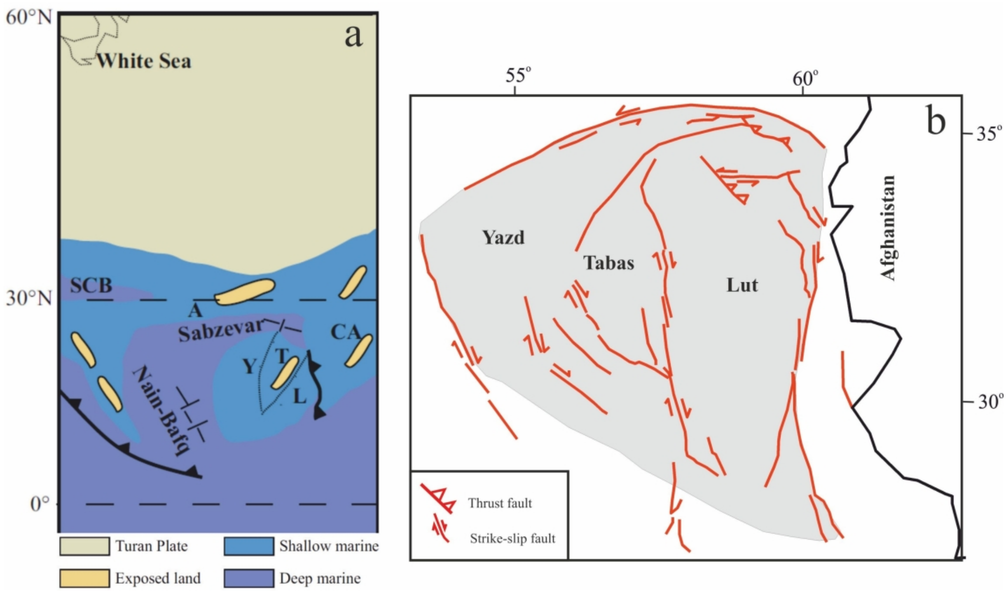

Fig. 14

252x148mm (300 x 300 DPI)

Highlights

- We reported the new age and geochemical data of Khur region and also compile all data from the magmatic rocks to consolidate our knowledge about the Late Cretaceous-Oligocene magmatism in the Lut block.
- The Late Cretaceous-Oligocene I-type granitoids in the Lut Block are characteristically high-K calcalkaline to slightly shoshonitic.
- Magmas likely formed by partial melting of a subduction-modified upper mantle in a syn to post-collisional extension-related zone due to the closure of the Sistan Sea between the Lut and Afghan Blocks and synchronous with rotation of the Lut Block.

Table 1. Whole-rock major and trace element compositions of volcanic and intrusive rocks of Khur area.

Sample	SH4	SH5	SH8	SH19	SH33	CH3	CH5	CH16	CH19
X	58°23′31″	58°23′33″	58°22′54″	58°23′32″	58°21′10″	58°25′10″	58°25′25″	58° 24′ 21″	58°24′ 30″
Y	33°3′ 12″	33° 3′ 1″	33°4′ 5″	33°2′ 3″	33°2′ 53″	33°9′ 19.3″	33°9′ 18″	33° 11′ 52″	33° 13′ 13″
Type	Ta	Ta	Ta	Ta	Ta	D	D	Ba	A
Wt.%									
SiO_2	56.52	55.76	57.63	60.17	55.47	63.11	63.73	55.13	60.81
TiO_2	1.64	1.68	1.57	1.08	1.76	0.51	0.45	0.96	0.67
Al_2O_3	16.1	16.28	16.06	15.59	16.25	17.09	16.98	16.75	15.34
TFeO	7.56	7.76	6.35	6.06	7.05	4.34	3.9	7.5	5.37
MnO	0.13	0.16	0.12	0.11	0.15	0.08	0.05	0.15	0.1
MgO	2.41	2.09	2.21	1.88	2.38	1.23	1.64	4.3	3.49
CaO	5.85	6.03	5.59	4.95	6.14	3.88	3.31	7.29	4.79
Na_2O	3.2	3.18	3.31	3.24	3.05	2.98	2.82	3.06	3.42
K_2O	3.47	3.68	3.47	3.84	3.68	2.92	3.01	2.46	3.13
P_2O_5	0.98	1	1.01	0.62	0.92	0.21	0.18	0.32	0.16
LOI	1.05	1.26	1.73	1.55	2.11	3	3.33	0.96	1.85
Total	98.91	98.88	99.05	99.09	98.96	99.35	99.4	98.88	99.13
ppm									
Ba	515	514	490	581	515	467	469	655	867
Be	4	3	4	4	3	2	3	1	<1
Co	18.3	18.9	17.1	12.5	17.0	5.5	5.1	16.8	27.5
Cs	4.8	7.3	5.5	6.4	3.8	4.1	2.8	1.9	2.1
Ga	18.5	18.6	17.7	18.5	19.0	17.1	16.1	15.5	16.5
Hf	9.1	9.2	9.0	8.5	9.2	4.1	4.1	3.3	3.5
Nb	15.4	15.1	15.2	14.3	16.6	7.0	7.0	8.6	7.1
Rb	158.6	179.7	156.1	169.4	150.0	96.6	98.5	74.8	69.4
Sn	3	3	3	2	3	1	<1	1	<1

Sr	401.1	419.6	388.6	400.6	408.6	368.7	338.9	613.6	1135.0
Ta	0.9	1.2	1.1	0.9	1.1	0.4	0.5	0.5	0.6
Th	19.9	20.9	20.2	18.4	20.5	9.7	9.7	7.4	9.8
U	4.9	4.9	5.0	4.6	4.8	2.4	2.7	3.6	2.5
V	176	179	162	99	176	42	66	114	250
W	1.7	2.2	2.6	2.5	2.3	1.4	1.4	1.4	0.8
Zr	385.9	398.5	389.9	360.0	400.2	160.9	156.7	130.5	123.1
Y	45.3	49.5	43.7	39.1	48.1	10.7	10.8	13.0	20.4
La	52.6	52.5	52.6	46.2	54.0	27.1	26.9	21.7	33.9
Ce	105.3	110.7	106.8	94.0	109.8	55.8	55.2	39.4	69.3
Pr	12.50	13.00	12.44	10.74	13.00	6.03	5.99	4.25	7.83
Nd	48.0	52.6	50.1	41.7	52.8	22.5	23.5	15.9	31.7
Sm	9.81	10.62	9.92	8.15	10.34	4.21	4.20	2.84	6.32
Eu	2.23	2.34	2.17	1.94	2.25	1.04	1.00	0.80	1.55
Gd	9.50	9.59	9.01	7.60	9.55	3.33	3.21	2.61	5.12
Tb	1.53	1.53	1.43	1.24	1.51	0.47	0.46	0.40	0.72
Dy	8.60	8.75	8.37	7.26	8.62	2.31	2.50	2.21	4.13
Er	5.10	5.29	4.82	4.48	5.10	1.10	1.21	1.37	2.20
Tm	0.76	0.79	0.71	0.64	0.75	0.14	0.16	0.18	0.34
Yb	5.02	5.08	4.40	4.21	4.96	0.95	1.07	1.40	2.36
Lu	0.74	0.79	0.70	0.67	0.74	0.15	0.14	0.21	0.34
Ratios									
*Eu/Eu	0.706	0.709	0.702	0.754	0.692	0.849	0.833	0.898	0.833
$(La/Yb)_N$	7.064	6.968	8.06	7.399	7.34	19.232	16.949	10.45	9.684

Table 1 *(continued)*

Sample	CH31	SH6	SH11	SH35	SH36	SH67	H14	H10
X	58° 24′ 8″	58°22′15″	58°22′18″	58°23′7″	58°22′2″	58°24′1″	58°26′39″	58°26′41″
Y	33° 11′ 41″	33°3′ 55″	33°3′ 27″	33°2′9″	33°2′6″	33°2′7″	33°7′25″	33°7′3″
Type	A	Mz	Mz	Mz	Mz	Mz	Di	Di

Wt.%								
SiO_2	59.18	55.12	55.91	56.92	56.05	56.28	62.18	58.02
TiO_2	0.84	1.7	1.6	1.35	1.45	1.58	0.76	0.96
Al_2O_3	16.05	16.36	17.11	17.35	16.44	16.53	15.77	16.21
TFeO	6.59	8.34	7.91	7.13	7.46	7.83	5.47	6.46
MnO	0.14	0.14	0.12	0.1	0.09	0.1	0.15	0.13
MgO	3.94	2.63	2.37	2.2	2.54	2.46	1.97	3.36
CaO	6.17	5.94	6.12	5.84	6.19	5.90	5.65	6.97
Na_2O	3.05	3.18	3.35	3.42	3.26	3.36	2.99	3.64
K_2O	2.59	3.79	3.68	3.6	3.61	3.70	2.9	1.19
P_2O_5	0.19	0.97	0.91	0.81	0.92	0.90	0.21	0.38
LOI	0.28	1.59	0.85	1.05	1.76	1.23	1.76	1.76
Total	99.02	99.76	99.93	99.77	99.77	99.87	99.81	99.81
ppm								
Ba	581	507	487	436	409	445	276	330
Be	<1	3	5	7	1	6	<1	3
Co	23.2	18.1	18.6	15.0	16.9	17.3	16.0	23.6
Cs	2.4	4.5	3.7	4.1	3.1	4.2	15.0	19.6
Ga	16.3	18.8	18.65	17.9	18.5	18.23	15.0	14.2
Hf	3.5	9.1	8.6	7.6	7.0	7.9	3.8	4.1
Nb	7.9	16.1	13.2	12.0	12.3	14.6	6.1	7.2
Rb	70.5	155.9	136.7	125.2	121.7	149.8	66.7	50.3
Sn	1	2	2	2	2	2	2	1
Sr	699.4	389.8	426.7	446.2	441.8	435.2	393.7	478.6
Ta	0.6	1.0	0.9	0.8	0.7	0.7	0.4	0.5
Th	6.9	19.6	18.5	15.0	15.1	17.4	8.3	8.5
U	2.1	4.9	3.7	3.5	3.4	4.2	1.9	1.9
V	160	166	137	130	143	159	112	163
W	0.7	2.1	2/0	1.7	1.5	1.9	1.1	1.5
Zr	134.6	381.3	325.7	313.9	305.3	339.5	156.3	178.8
Y	16.3	42.9	38.9	36.5	34.4	41.3	16.3	19.4
La	21.3	52.7	50.4	41.6	40.6	45.7	20.4	24.1
Ce	43.9	104.6	98.5	84.5	82.2	87.1	37.7	48.0
Pr	4.91	12.46	10.84	9.88	9.47	9.59	4.35	5.33

Nd	19.3	48.0	37.4	38.3	36.7	38.7	17.0	20.8
Sm	3.83	9.63	9.57	7.98	7.52	8.63	3.21	4.27
Eu	1.09	2.13	2.10	1.90	1.87	1.95	1.04	1.22
Gd	3.66	8.92	8.67	7.64	7.48	7.87	3.14	4.03
Tb	0.56	1.47	1.36	1.15	1.09	1.29	0.48	0.67
Dy	3.36	7.77	6.81	6.74	6.66	7.39	2.64	3.79
Er	2.05	4.75	4.16	4.05	3.46	4.37	1.55	2.18
Tm	0.30	0.67	0.56	0.58	0.52	0.63	0.23	0.34
Yb	2.04	4.59	4.25	3.61	3.56	3.78	1.62	2.17
Lu	0.30	0.70	0.65	0.58	0.55	0.59	0.24	0.35
Ratios								
*Eu/Eu	0.89	0.703	0.709	0.744	0.762	0.735	1.002	0.899
$(La/Yb)_N$	7.039	7.741	7.753	7.769	7.689	7.675	8.49	7.488

Table 1 *(continued)*

Sample	D4	D5	D9	D16	D23	D24	D32	D33	D69
X	58°29′15″	58°29′5″	58°29′36″	58°28′46″	58°29′40″	58°29′29″	58°29′35″	58°29′46″	58°28′56″
Y	33°4′34″	33°2′55″	33°3′7″	33°3′20″	33°3′31″	33°3′36″	33°2′39″	33°4′18″	33°5′16″
Petrography	Di	Gr	Gd	Gd	G	Gd	Di	Gr	Gd
Wt. %									
SiO_2	58.42	61.82	54.23	54.6	49.68	53.77	64.95	67.69	54.39
TiO_2	0.99	0.65	1.02	1.01	1.02	0.93	0.64	0.34	1.14
Al_2O_3	16.1	15.28	15.62	16.99	15.32	17.9	15.18	15.3	16.26
FeOt	7.09	5	7.85	7.16	9.4	8	5.33	3.4	8.76
MnO	0.13	0.08	0.15	0.12	0.15	0.15	0.09	0.09	0.14
MgO	3.32	3.2	4.96	4.77	8.35	4.11	1.72	0.95	4.49
CaO	6.04	4.85	8.55	7.81	9.48	9.17	4.85	3.92	7.55
Na_2O	2.5	3.23	2.41	3.16	2.08	2.84	3.02	3.39	2.79
K_2O	3.18	3.68	2.56	1.84	1.6	2.12	2.95	3.08	2.34
P_2O_5	0.33	0.21	0.32	0.3	0.36	0.43	0.33	0.19	0.34
LOI	1.7	1.83	2.15	2.05	2.38	0.4	0.75	1.49	1.59

Total	99.8	99.83	99.82	99.81	99.82	99.82	99.81	99.84	99.79
ppm									
Ba	311	347	421	306	250	325	511	509	391
Be	<1	<1	<1	<1	2	2	1	<1	1
Co	21.6	10.6	27.8	22.9	32.5	25.5	7.2	3.3	27.4
Cs	12.7	1.3	2.3	1.3	0.6	4.3	1.8	2.6	3.7
Ga	15.2	14.1	16.1	15.2	14.3	15.8	13.5	13.0	16.4
Hf	4.4	4.2	3.3	3.5	2.9	3.0	4.1	3.8	5.2
Nb	7.6	5.6	5.1	8.3	3.9	4.4	8.6	7.0	9.7
Rb	66.6	42.6	71.2	52.8	27.8	52.0	85.2	108.6	56.4
Sn	1	2	1	1	<1	<1	<1	1	2
Sr	466.6	410.3	552.4	450.6	472.0	533.2	417.6	425.7	519.4
Ta	0.6	0.6	0.3	0.7	0.2	0.3	0.6	0.6	0.6
Th	9.1	9.9	8.0	6.7	4.5	6.2	7.2	10.4	12.1
U	1.9	2.7	1.9	1.7	1.0	1.4	2.0	3.0	3.0
V	172	110	246	240	227	261	85	34	230
W	0.9	1.1	1.0	0.5	<0.5	0.8	2.7	1.3	1.7
Zr	184.3	165.7	129.3	157.1	109.0	114.9	161.5	167.4	195.2
Y	18.7	14.8	22.2	19.2	20.0	20.4	19.1	14.0	26.7
La	25.1	19.0	22.7	19.6	16.9	17.6	23.5	24.7	29.9
Ce	49.8	38.4	49.7	39.3	32.5	35.5	46.6	44.3	60.1
Pr	5.50	4.15	5.89	4.52	3.99	4.22	5.27	4.88	7.07
Nd	22.1	16.3	24.6	17.7	16.9	19.3	20.6	18.3	28.7
Sm	4.43	2.97	5.73	3.99	3.61	3.76	3.84	2.96	5.60
Eu	1.20	0.82	1.48	1.05	1.14	1.23	1.12	0.84	1.38
Gd	3.98	2.87	4.71	3.80	3.86	4.09	3.83	2.59	5.91
Tb	0.65	0.47	0.79	0.66	0.63	0.64	0.61	0.40	0.86
Dy	3.73	2.77	4.11	4.02	3.75	3.85	3.52	2.52	5.22
Er	2.22	1.59	2.46	2.29	2.23	2.31	2.23	1.60	2.90
Tm	0.33	0.24	0.37	0.37	0.32	0.34	0.34	0.24	0.44
Yb	2.06	1.48	2.26	2.29	2.12	2.14	2.20	1.91	2.83
Lu	0.33	0.24	0.34	0.35	0.33	0.31	0.35	0.29	0.40
Ratios									
*Eu/Eu	0.874	0.859	0.871	0.825	0.934	0.959	0.893	0.928	0.733

$(La/Yb)_N$	8.215	8.655	6.772	5.77	5.374	5.545	7.202	8.719	7.123

Abbreviations: R: Rhyodacite, D: Dacite, A: Andesite, Ta: Trachyandesite, Ba: Basaltic andesite, G: Gabbro, Gd: Gabbrodiorite, Mz: Monzonite, Di: Diorite, Gr: Granodiorite, LOI: Loss on Ignition.

Table 2. Rb–Sr and Sm–Nd isotopic data of eleven whole-rock samples from the Khur area.

Sampl	Sr	Rb	^{87}Rb/^{8}	Error	^{87}Sr/^{86}S	Error	(^{87}Sr/^{86}S	Nd	Sm	^{147}Sm/^{1}	Error		Error	εNdi
D4	467	67	0.415	0.012	0.70510	0.00002	0.70484	22.1	4.4	0.120	0.00	0.512774	0.0000	+3.1
D23	472	27	0.170	0.005	0.70485	0.00002	0.70475	16.9	3.6	0.129	0.00	0.512733	0.0000	+2.2
D24	533	52	0.282	0.008	0.70492	0.00001	0.70476	19.3	3.8	0.118	0.00	0.512702	0.0000	+1.6
D32	418	85	0.588	0.017	0.70512	0.00002	0.70479	20.6	3.8	0.112	0.00	0.512773	0.0000	+3.1
D33	426	109	0.738	0.021	0.70540	0.00001	0.70498	18.3	3.0	0.098	0.00	0.512631	0.0000	+0.3
SH6	390	156	1.156	0.033	0.70545	0.00002	0.70479	-	-	-	-	-	-	-
SH35	446	125	0.812	0.023	0.70524	0.00002	0.70478	38.3	8.0	0.126	0.00	0.512782	0.0000	+3.1
CH16	113	69	0.177	0.005	0.70506	0.00002	0.70496	31.7	6.3	0.121	0.00	0.512656	0.0000	+0.7
SH4	420	180	1.238	0.035	0.70540	0.00002	0.70469	52.6	10.	0.122	0.00	0.512772	0.0000	+3.0
SH5	401	159	1.144	0.032	0.70563	0.00002	0.70498	48.0	9.8	0.124	0.00	0.512759	0.0000	+2.7
SH19	409	150	1.061	0.030	0.70546	0.00002	0.70485	52.8	10.	0.118	0.00	0.512710	0.0000	+1.8

Note: ^{87}Rb decay λ = 1.3972 × 10^{-11} a^{-1} (Villa et al., 2015); ^{147}Sm decay (Steiger and Jager, 1977λ = 6.54 × 10^{-12} a^{-1}; The ^{143}Nd/^{144}Nd and ^{147}Sm/^{144}Nd ratios of chondrite at present day are 0.512638 and 0.1967, respectively (Jacobsen and Wasserburg, 1980).

Table 3. Results of U–Pb–Th the laser-ablation multicollector ICP mass spectrometry analysis of zircon from dike of diorite and monzonite.

Spot	U (ppm)	$^{206}Pb/^{204}Pb$	U/Th	$^{206}Pb/^{207}Pb$	± (%)	$^{207}Pb/^{235}U$	± (%)	$^{206}Pb/^{238}U$	± (%)	$^{206}Pb/^{238}U$ (Ma)	± (Ma)
D45- 36	300	19712	1.9	20.2087	2.3	0.0471	3.6	0.0069	2.7	44.4	1.2
D45- 37	156	3690	1.6	21.3277	2.8	0.0448	4.0	0.0069	2.8	44.5	1.2
D45- 38	273	2416	2.0	22.6357	2.9	0.0425	4.0	0.0070	2.7	44.8	1.2
D45- 39	212	4213	1.4	23.2514	3.0	0.0402	4.1	0.0068	2.9	43.6	1.3
D45- 40	571	2676	2.0	22.2960	1.6	0.0429	3.3	0.0069	2.8	44.6	1.3
D45- 41	69	1584	1.4	25.0079	8.6	0.0386	9.1	0.0070	3.2	45.0	1.4
D45- 42	452	6224	2.2	21.1039	2.0	0.0462	3.3	0.0071	2.6	45.5	1.2
D45- 43	259	1964	1.5	25.1790	3.2	0.0384	4.4	0.0070	2.9	45.1	1.3
D45- 44	633	20274	1.7	21.0806	1.5	0.0477	3.1	0.0073	2.7	46.8	1.2
D45- 45	470	3055	2.0	13.2226	5.6	0.0753	6.9	0.0072	4.0	46.4	1.9
D45- 46	472	11564	1.5	20.4629	1.8	0.0465	3.4	0.0069	2.9	44.4	1.3
D45- 47	1130	18579	1.1	21.2615	1.4	0.0441	6.3	0.0068	6.1	43.7	2.7
D45- 48	933	61129	1.7	18.6315	1.6	0.0525	3.2	0.0071	2.8	45.6	1.3
Monzonite											
SH6-1	226	1930	1.4	15.3936	5.1	0.0545	5.1	0.0061	3.8	39.1	1.3
SH6-2	265	36627	1.2	18.5838	2.4	0.0464	3.9	0.0064	3.0	42.6	1.3
SH6-3	187	21935	1.0	21.6323	3.1	0.0409	3.5	0.0064	3.2	41.1	1.4
SH6-4	315	60035	1.4	20.0623	2.1	0.0444	2.3	0.0064	2.5	41.4	1.3
SH6-5	276	23145	1.0	21.7221	3.2	0.0408	3.4	0.0063	3.1	41.2	1.5
SH6-6	259	37891	1.2	21.5326	3.7	0.0401	3.1	0.0063	2.9	40.3	2.2
SH6-7	463	29863	1.0	19.8436	3/8	0.0415	3.2	0/0063	2.9	39.3	0.9
SH6-8	258	95245	0.9	21.7223	2.4	0.0410	3.4	0.0064	4.1	41.3	2.0
SH6-9	465	128786	1.0	20.3438	2.4	0.0420	3.8	0.0062	3.7	39.6	2.1
SH6-10	297	1367	0.9	17.8336	3.6	0.0424	2.8	0.0063	3/6	40.3	4.1

SH6-11	1678	12571	0.7	20.2623	2.3	0.0453	3.4	0.0066	2.7	42.6	1.5
SH6-12	783	203467	3.7	17.6236	2.1	0.6729	1.7	0.0864	3.6	527.4	12.5
SH6-13	345	25612	5.9	17.1456	0.8	0.6918	1.1	0.0849	3.1	530.2	14.3
SH6-14	287	115431	3.6	17.6323	1.2	0.7387	1.3	0.0887	2.2	553.9	14.1
SH6-15	253	12463	6.8	17.3923	1.1	0.7412	1.2	0.0925	2.3	572.6	14.0
SH6-16	367	63467	1.8	17.0063	1.2	0.7213	1.4	0.0886	3.2	546.3	14.9
SH6-17	451	29345	1.4	19.3263	1.3	0.7132	1.5	0.0880	1.1	543.1	4.9
SH6-18	542	29763	2.4	17.0345	2.1	0.7161	3.1	0/0883	3.7	545.9	17.1
SH6-19	678	56934	1.5	17.0698	0.9	0.7056	1.4	0/0873	1.1	541.2	5.7
SH6-20	467	43754	2.3	17.0389	1.1	0.7067	1.5	0/0874	1.3	539.2	7.1

Table 4. U–Pb data obtained by ID-TIMS from zircon in dike of granodiorite (sample CH4).

zircon type	U (ppm)	Th/U	^{206}Pb/^{204}Pb	^{207}Pb/^{235}U	2 sigma	^{206}Pb/^{238}U	2 sigma	Rho	^{207}Pb/^{206}Pb	2 sigma	^{206}Pb/^{238}U [Ma]	2 sigma [Ma]	^{207}Pb/^{235}U [Ma]	2 sigma [Ma]	Disc. (%)	zircon type	U (ppm)
tip	124	0.20	60	0.03876	0.00481	0.00635	0.00007	0.36	0.04427	0.00533	40.8	0.5	38.6	4.7	0.0	176.4	2.3
short prisms	219	0.53	54	0.11810	0.00863	0.01364	0.00015	0.08	0.06279	0.00458	87.3	1.0	113.3	7.8	701.1	148.2	88.1
short prisms	131	0.39	341	0.07960	0.00111	0.01130	0.00004	0.39	0.05109	0.00067	72.4	0.2	77.8	1.0	244.7	29.8	70.8
short prisms	205	0.32	42	0.29333	0.01921	0.02002	0.00032	0.13	0.10628	0.00695	127.8	2.1	261.2	15.0	1736.5	115.4	93.5
short prisms	148	0.49	3114	0.77831	0.00208	0.05159	0.00011	0.86	0.10941	0.00015	324.3	0.7	584.5	1.2	1789.6	2.5	83.9
tip	70	0.20	134	0.08684	0.00260	0.01104	0.00006	0.28	0.05704	0.00165	70.8	0.4	84.6	2.4	493.2	62.6	86.1
tip	352	0.27	971	0.38102	0.00220	0.05097	0.00014	0.57	0.05422	0.00027	320.5	0.9	327.8	1.7	380.1	11.2	16.1

Explanation: Rho is the correlation between the $^{206}Pb/^{238}U$ and $^{207}Pb/^{235}U$ ratios; 2 sigma uncertainties are calculated by propagating the uncertainties from measurement, fractionation, blank correction and common Pb correction.